Deanship of Graduation Studies

Al-Quds University

An accelerating algorithm for the computation of electromagnetic scattering from 3D scatterers

Noor Majed Mohammad Obead

M.Sc. Thesis

Jerusalem – Palestine

1439/2018

An accelerating algorithm for the computation of electromagnetic scattering from 3D scatterers

Prepared By:
Noor Majed Mohammad Obead

B.Sc. :Communication Engineering and Technology,
Palestine Technical University-PTUK, Palestine

Supervisor: Dr. Mohammad Kouali

A thesis Submitted in Partial Fulfillment of the Requirements for the Degree of Master of Electronic and Computer Engineering, At Al-Quds University

1439/2018

Al-Quds University

Deanship of Graduate Studies

Master of Electronic and Computer Engineering

Thesis Approval

An accelerating algorithm for the computation of electromagnetic scattering from 3D scatterers

Prepared By: Noor Majed Mohammad Obead

Registration No. :21511703

Supervisor: Dr. Mohammad Kouali

Master thesis submitted and accepted. Date: 4 / 8 /2018

The names and signatures of the examining committee members are as follows:

1- Head of Committee: Mohammad Kouali Signature:.....
2- Internal Examiner: Ahmed Abdu Signature:.....
3- External Examiner: Atalla Balalem Signature:.....

Jerusalem – Palestine

1439 – 2018

Declaration

I Certify that this thesis submitted for the degree of master is the result of my own research, except where otherwise acknowledged, and that this thesis (or any part of the same) has not been submitted for a higher degree to any other university or institution.

Signed: .....

Noor Majed Mohammad Obead

Date: 3-6-2018

Dedication

This work is dedicated to my family and my friends who supported me all the time.

Noor Majed Obead

Acknowledgments

I would first like to thank my thesis supervisor Dr. Mohammad Kouali. The door to Dr. Mohammad was always open whenever I ran into a trouble spot or had a question about my research and writing.
Also I would like to thank the thesis examiner Dr. Ahmed Abdu and Dr. Atalla Balalem for their valuable suggestions and corrections on this work.
Special thanks to my friends Shrouq Ahmed, Mays'a Abu-Shams, and Abd-Elbasset Laifaoui for their endless support.
Finally, I must express my very profound gratitude to my parents and to my family for providing me with unfailing support and continuous encouragement throughout my years of study and through the process of researching and writing this thesis. This accomplishment would not have been possible without them. Thank you.

Contents

Declaration i

Dedication ii

Acknowledgement iii

Contents iv

List of Figures vii

Glossary and Abbreviations xi

Abstract xiii

1 Introduction 1

1.1 Motivation 1

1.2 Problem statement 2

1.3 Thesis Goals 2

1.4 Thesis Contribution 2

1.5 Computational Electromagnetic Methods 3

1.5.1 Finite Difference Time Domain Method . . 4

1.5.2 Finite Element Method 4

1.5.3 Method of Moment 5

1.5.4 Geometrical Theory of Diffraction 5

1.5.5 Physical Optics 6

1.6 Computational methods for two scatterers 6

1.7 Thesis Organization 8

2 Electromagnetic Waves and Computational Methods 10

2.1 Maxwell's Equations 10
2.2 Electromagnetic Boundary Conditions 11
2.3 Wave propagation and plan waves 13
2.4 Green's Function 16
2.5 Huygen's Principle and Extinction Theorem . . . 17
2.6 Spherical Coordinates 19
2.7 Diffraction Matrix 21
2.8 Radar Cross Section (RCS) 22
2.9 Conclusion 25

3 Electromagnetic Scattering From Single Scatterer 26

3.1 Integral Equations 26
3.2 Method of Moment (MoM) 27
3.2.1 Charged thin wire 29
3.2.2 Charged plate 34
3.2.3 Method of Moments applied for scattering problem (Scattering from Plate) 36
3.2.4 Rough surface 42
3.3 Conclusion 46

4 Electromagnetic Scattering from Two Scatter-

ers **48**

4.1 Integral Equations for two scatterers 49

4.2 Discretization by Method of Moment 51

4.3 Extended Propagation Inside Layer Expansion (E-PILE) 54

4.4 Physical Optics 62

4.5 Adaptive Cross Approximation 70

4.6 Conclusion 76

5 Conclusion and Future Work **79**

5.1 Conclusion 79

5.2 Future Work 80

Bibliography **81**

List of Figures

2.1 The domain Ω_0 is bounded by the contour $C_{0,\infty}$ and the surface S whereas Ω_1 is bounded by the contour $C_{1,\infty}$ and the surface S. 17

2.2 Illustration of spherical coordinates polarization bases used in transmission and reception. 19

2.3 Near and Far field geometry. 23

3.1 A thin conductive wire with length L. 29

3.2 The line divided to segments of length Δx. . . . 30

3.3 Charge distribution on a wire of length = 1 m and radius = 0.001 m when applying voltage potential of 1 V, the wire is divided into 10 segments using MoM. 34

3.4 Charge distribution on a wire of length = 1 m and radius = 0.001 m when applying voltage potential of 1 V, the wire is divided into 100 segments using MoM. 34

3.5 Square plate of length L discretized to small square patches each of length $2a$. 35

3.6 The computed surface charge density of square plate of length 1 m, with 10 segments using MoM 37

3.7 The computed surface charge density of square plate of length 1 m, with 100 segments using MoM 37

3.8 The geometry of the problem: the excitation of square plat by plane wave. 41

3.9 Comparison of the RCS from MoM and the results from FEKO for horizontal polarization, the square plate has dimensions $10\lambda_0 \times 10\lambda_0$, $\Delta x = \Delta y = \lambda_0/8$ $\theta_i = 0^o$, $\phi_i = 0^o$. 42

3.10 Current distribution and the RCS from square plate of dimension $10\lambda_0 \times 10\lambda_0$. 43

3.11 Comparison of the RCS from MoM and the results from FEKO for TE polarization, the square plate has dimensions $10\lambda_0 \times 10\lambda_0$, $\Delta x = \Delta y = \lambda_0/8$ $\theta_i = 0^o$, $\phi_i = 0^o$. 44

3.12 The geometry of the problem: the excitation of rough surface by plane wave. 44

3.13 Comparison of the RCS from MoM and the results from FEKO for horizontal polarization, the rough surface has dimensions $8\lambda_0 \times 8\lambda_0$, $\Delta x = \Delta y = \lambda_0/8$ $\theta_i = 0^o$, $\phi_i = 0^o$. 46

3.14 Comparison of the RCS from MoM and the results from FEKO for a vertical polarization, the rough surface has dimensions $8\lambda_0 \times 8\lambda_0$, $\Delta x = \Delta y = \lambda_0/8$ $\theta_i = 0^o$, $\phi_i = 0^o$. 47

4.1 Two scatterers located in volume V_0 50

4.2 Physical interpretation of E-PILE method. 58

4.3 The geometry of two parallel plates. 59

4.4 The RCS for two parallel plates computed by MoM-LU and E-PILE of order 0, 3 and 8, the plates are at dimensions of $2\lambda_0 \times 2\lambda_0$ and $6\lambda_0 \times 6\lambda_0$, separated by distance of $5\lambda_0$, and illuminated by plane wave at an incident angle of $\theta_i = 0^o$. 60

4.5 The RCS for two parallel plates computed by MoM-LU and E-PILE of order 0, 3 and 8, the plates are at dimensions of $2\lambda_0 \times 2\lambda_0$ and $6\lambda_0 \times 6\lambda_0$, separated by distance of $5\lambda_0$, and illuminated by plane wave at an incident angle of $\theta_i = 45^o$. 61

4.6 The geometry of square plate above rough surface. 62

4.7 The RCS of plate above rough surface computed by MoM-LU and E-PILE of order 0, 3 and 8, the two scatterers are at dimensions of $2\lambda_0 \times 2\lambda_0$ and $8\lambda_0 \times 8\lambda_0$, separated by distance of $5\lambda_0$, and illuminated by plane wave at an incident angle of $\theta_i = 0^o$. 63

4.8 The RCS of plate above rough surface computed by MoM-LU and E-PILE of order 0, 3 and 8, the two scatterers are at dimensions of $2\lambda_0 \times 2\lambda_0$ and $8\lambda_0 \times 8\lambda_0$, separated by distance of $5\lambda_0$, and illuminated by plane wave at an incident angle of $\theta_i = 45^o$. 64

4.9 The excitation at the first scatterer by a plan wave. 66

4.10 The excitation at the second scatterer by a plan wave. 68

4.11 The RCS of plate above rough surface computed by MoM-LU, E-PILE, and E-PILE+PO1+PO2, the two scatterers are at dimensions of $1\lambda_0 \times 1\lambda_0$ and $8\lambda_0 \times 8\lambda_0$, separated by distance of $5\lambda_0$, and illuminated by plane wave at an incident angle of $\theta_i = 0^o$. 70

4.12 The RCS of plate above rough surface computed by MoM-LU, E-PILE+PO1+PO2 and and the proposed method E-PILE+PO1+PO2+ACA. The two scatterers are at dimensions of $1\lambda_0 \times 1\lambda_0$ and $8\lambda_0 \times 8\lambda_0$, separated by distance of $5\lambda_0$, and illuminated by a horizontally polarized plane wave at an incident angle of $\theta_i = 0^o$. 75

4.13 The RCS of plate above rough surface computed by MoM-LU, E-PILE+PO1+PO2 and the proposed method E-PILE+PO1+PO2+ACA. The two scatterers are at dimensions of $1\lambda_0 \times 1\lambda_0$ and $8\lambda_0 \times 8\lambda_0$, separated by distance of $5\lambda_0$, and illuminated by a horizontally polarized plane wave at an incident angle of $\theta_i = 45^o$. 76

4.14 The RCS of plate above rough surface computed by MoM-LU, E-PILE +PO1 +PO2 and and the proposed method E-PILE +PO1 +PO2 +ACA. The two scatterers are at dimensions of $1\lambda_0 \times 1\lambda_0$ and $8\lambda_0 \times 8\lambda_0$, separated by distance of $5\lambda_0$, and illuminated by a vertically polarized plane wave at an incident angle of $\theta_i = 45^o$. 77

4.15 Comparison of time requires for the three methods, MoM-LU, E-PILE combined with PO and E-PILE combined with PO accelerated by ACA. The time is for scenario of square plate of dimensions from $1\lambda_0 \times 1\lambda_0$ to $4\lambda_0 \times 4\lambda_0$ and the rough surface is in the dimension of $5\lambda_0 \times 5\lambda_0$. 78

List of Acronyms

ACA : Adaptive Cross Approximation

CMBA : Complex Multipole Beam Approach

E-PILE : Extended - Propagation Inside Layer Expansion

FB-SA : Forward - Backward with Spectral Acceleration

FDTD : Finite Difference Time-Domain

FEM : Finite Element Method

IE: Integral Equation

IML : Impedance Matrix Localization method

GTD : Geometrical Theory of Diffraction

KA : Kirchoff Approximation

LHI : Linear, Homogeneous and Isotropic

MFIE : Magnetic field integral equation

MoM : Method of Moment

MoM-LU : Method of Moment - lower Upper

PDM : Perfect Dielectric Medium

PEC : Perfect Electric Conductor

PILE : Propagation Inside Layer Expansion

PMC : Perfect Magnetic Conductor

PO : Physical Optics

RCS : Radar Cross Section

Abstract

Method of Moment (MoM) is one of the well-known methods to solve the scattering equations. This method is applied for one scatterer or a very small scenarios of two scatterers. MoM uses huge memory resources and long time to solve the system, that make this method limited to small electrical problems.

In order to solve the system of MoM efficiently, many supported methods appear, Extended- Propagation Inside Layer Expansion (E-PILE) proposed an attractive method to solve the system provided by MoM. Also, many accelerating methods have appeared, Physical Optics(PO) approximates the surface current on both scatterers, this approximation dramatically reduces the complexity of the computations. More over, Adaptive Cross Approximation (ACA) also proposed algebraic algorithm greatly helps to approximate a large matrix, the new approximated matrix is easily used and saved.

In this thesis, we propose a hybrid method that uses MoM to descritize the problem of two 3D scatterers, then PO approximation is applied to calculate the local interaction at the two 3D scatterers. After that, ACA is combined to accelerate calculations of the coupling occurs between the two scatterers. The proposed method is then applied on a scenario of a square plate located above rough surface. The proposed method (E-PILE+PO+ACA) has successfully reduced the complexity of the system and the required computation time, the simulations show

an acceptable results with much reduced time, that make this proposed method suitable for scenarios of large sizes.

Chapter 1

Introduction

In this chapter, the motivation of this thesis and the problem statement will be discussed. Then we will talk about the goals of the topic and the contribution of our proposed method.

1.1 Motivation

Recently, scattering theorem has attracted more attention from researchers. In general, scattering phenomenon used to refers to several cases in a way such that propagating wave hits an object then it is reflected, distorted, transmitted or in general "scattered ". The importance of this scattered wave is that it contains information about the object it hits. These scattered waves can be processed in many ways, and the results could be used in many applications like radar and remote sensing, material science, biology and medical applications, etc, that was the main motivation to study this phenomenon. Few decays ago, it was so difficult to make deep studies in this field, because of its expensive requirements (memory, computation time), but thanks to the fast developments of computers, which allowed us to apply exact methods and then make some approximations or test new methods to accelerate its computa-

tions. Since the scattering phenomenon has several applications, there is special attention to know its complete solution, the need for a 3D solution for the problem becomes necessary and depends on the applications deal with that phenomenon.

1.2 Problem statement

The exact methods used to solve scattering problem from two 3D scatterers are limited to the size of the geometry used. Hybridization of an exact method with some approximated methods lead to acceptable results with reduced requirements such as the memory and time, but still limited to small geometry sizes.

1.3 Thesis Goals

This thesis aims to solve 3D scattering problem with an efficient method, this method reduces both the complexity of the system and the required time to solve the scattering equations, and apply it for two 3D scatterers (object above rough surface).

1.4 Thesis Contribution

This thesis proposes an accelerated hybrid method, the method capable to solve scattering problem for two large size 3D scatterers, with reduc-

tion in memory and computation time with an acceptable error rate.

1.5 Computational Electromagnetic Methods

As can be expected from the previous sections, solving the electromagnetic equations directly is analytically impossible. So, many methods are found to solve these equations, each method has its own strong and weak points, also, these methods are divided to two main classes, exact method which sometimes called low-frequency methods, and the approximate methods which are known as high-frequency methods.

Exact methods (low-frequency methods) solve Maxwell equations directly without approximations. In general, the results of these methods can be used as a reference to the approximation methods. While low-frequency methods give the exact solutions, which is very important, they are limited to objects of very small sizes, because of its huge memory requirements and very long computation time. From this point, approximation methods (high frequency methods) take its importance, since these methods give some approximations on solving Maxwell equations, noticeable difference in memory requirements and computations time can be achieved.

Moreover, these methods can be classified to the time domain or frequency domain method. In this section, we would mention some of these methods and in the following chapters, and explain in details MoM as an

exact method, PO and ACA as two approximate methods to accelerate MoM.

1.5.1 Finite Difference Time Domain Method

The Finite Difference Time-Domain (FDTD) method [2, 3] uses the method of finite differences to solve Maxwell's Equations in the time domain. Application of the FDTD method is usually very straightforward: the solution domain is typically discretized into small rectangular or curvilinear elements. FDTD excels at analysis of inhomogeneous and non linear media, though its demands for system memory are high due to the discretization of the entire solution domain, and it suffers from dispersion issues. FDTD is applied in packaging and wave guide problems, as well as in the study of wave propagation in complex dielectrics.

1.5.2 Finite Element Method

The Finite Element Method (FEM) [4, 5] is a method used to solve frequency domain boundary valued electromagnetic problems by using a variational form. It can be used with two- and three-dimensional canonical elements of different shape, allowing for a highly accurate discretization of the solution domain. The FEM is often used in the frequency domain for computing the frequency field distribution in complex, closed regions such as cavities and wave guides. As in the FDTD method, the solution domain must be truncated, making the FEM unsuitable for ra-

diation or scattering problems unless combined with a boundary integral equation approach [4].

1.5.3 Method of Moment

The Method of Moments (MoM) [6] is a technique used to solve electromagnetic boundary or volume integral equations in the frequency domain. Because the electromagnetic sources are the quantities of interest, the MOM is very useful in solving radiation and scattering problems. In this thesis, we focus on the practical solution of boundary integral equations of radiation and scattering using this method (we will discuss it in details in chapter 3).

1.5.4 Geometrical Theory of Diffraction

The Geometrical Theory of Diffraction (GTD) [7, 8] uses ray-optics to determine electromagnetic wave propagation. The spreading, amplitude intensity and decay in a ray package are computed using from Fermat's principle and the radius of curvature at reflection points. The GTD attempts to account for the fields diffracted by edges, allowing for a calculation of the fields in shadow regions. The GTD is fast but often yields poor accuracy for more complex geometries.

1.5.5 Physical Optics

Physical optics (PO) [9] is a method for approximating the high-frequency surface currents, allowing a boundary integration to be performed to obtain the fields. As we will see, the PO and the MoM are used to solve the same integral equation, though the MoM calculates the surface currents directly instead of approximating them. However, PO does not take in account for the fields diffracted by edges or those from multiple reflections, so supplemental corrections are usually added to it. The PO method is used extensively in high-frequency (we will discuss it in chapter 4).

1.6 Computational methods for two scatterers

In the previous section, some exact and approximated methods were discussed to solve the scattering problem for one scatterer. Several applications deal with scenarios of two or more scatterers, the scattering problem becomes more huge and more complex, in this case the coupling between the scatterers must be taken in account. To solve the scattering problem in this case, some considered the scattering problem as a 2D problem, then many methods were proposed to solve the 2D scattering problem [10]-[18].

Other methods deal with the scattering problems as a three-dimensional problems [19]-[26]. As expected, it is significant for the practical appli-

cations to study the case of three dimension problems.

For large 3D problems, exact methods such as MoM are limited to the memory requirements. From that point, some methods proposed assumptions to simplify the calculations, for example, in [19] a hybrid method combines Kirchoff Approximation (KA) with MoM to study the scattering from 3D perfect electric conductor located above 2D dielectric rough surface. In [20], KA is used to derive a half-space Green function with the rough surface interface, the MoM is applied in a complete 3D problem.

The work in [22], [23] proposed some assumptions to compute the coupling between the scatterers from the four-path model. In [24],[25] a proposed method called Finite-Difference Time Domain (FDTD) approach to discuss the scattering of 3D object located above 2D rough surface. An efficient numerical PILE (Propagation-Inside-Layer Expansion) method for computing the field scattered by rough layers is proposed in [13], then it is extended to 3D problems in a proposed method called Extended-Propagation Inside Layer Expansion (E-PILE) in [14].

For a large scenario, [16] proposed method that combines E-PILE with FBSA method to calculate the local interaction on the rough surface and combined E-PILE with PO to compute the interaction on the object. Moreover, in [26] forward backward method is proposed to calculate the local interaction on the rough surface for 3D problem. Furthermore, there are other techniques to accelerate the computations like Complex

Multipole Beam Approach (CMBA)[27], this method uses a series of beams at the boundary instead of one beam, these beams are called Gabor functions, this combination reduces the size of the matrix, CMBA is combined with MoM in [28]. The Impedance Matrix Localization method (IML) is introduced in [29]. This technique introduces a new special basis functions and test functions. These functions localize the significant interactions and uses them, this method also reduces the required memory.

In[30], a proposed purely algebraic method called ACA to accelerate the electromagnetic computations of MoM, in [31] the ACA method is hybrid with E-PILE and FBSA to solve a 2D problem with huge number of unknowns.

Very recently, a bi-iteration model is proposed in [32], the model is expressed by outer iteration and inner iteration, the proposed model effectively solves the more complicated scattering problem from a 3D object located above a 2D rough surface than the common methods.

1.7 Thesis Organization

This thesis is organized as follows:

Chapter 2: Electromagnetic waves and computational methods. In this chapter, we discuss the basics of electromagnetics, main principles we used in the followed chapters.

Chapter 3: Electromagnetic scattering from a single scatterer. This chapter discusses MoM and solves the integral equations for one scatterer in the cases of electrostatic and scattering problems.

Chapter 4: Electromagnetic scattering from two 3D scatterers. In this chapter, MoM is applied for a geometry of two 3D scatterers, then approximated methods are combined (PO+ACA) to accelerate the computations of the scattering problem.

Chapter 5: Conclusion and future work. The conclusion of the whole thesis is discussed in this chapter with suggested future work.

Chapter 2

Electromagnetic Waves and Computational Methods

Solving the electromagnetic problems mainly depend on applying Maxwell's equations with some boundary conditions. In this chapter, we discuss part of Maxwell's equations, which we will use later, then wave equation as a result of solving Maxwell's equations is introduced. After that, we derive the Green's function, and also study Huygens principle and Extinction theory, then the far field of wave propagation and Radar Cross Section (RCS) is discussed.

2.1 Maxwell's Equations

James Clerk Maxwell published set of equations that describe the phenomenon of the electric field and the magmatic field. The relations between the different fields are given by [1]

$$\boldsymbol{\nabla} \cdot \mathbf{B} = 0, \tag{2.1}$$

$$\boldsymbol{\nabla} \times \mathbf{E} = -\frac{\partial}{\partial t}\mathbf{B}, \tag{2.2}$$

$$\boldsymbol{\nabla} \cdot \mathbf{D} = \rho, \tag{2.3}$$

$$\boldsymbol{\nabla} \times \mathbf{H} = \mathbf{J} + \frac{\partial}{\partial t}\mathbf{D}, \tag{2.4}$$

Where $\boldsymbol{\nabla}$ is the vector differential operator, **E, H** represent the electric field intensity and the magnetic field intensity measured in $V/m, A/m$ respectively, **D** is the electric flux density, **B** is the magnetic flux density,**J** is the current density. If the medium is Linear, Homogeneous and Isotropic (LHI), then [33]

$$\mathbf{D} = \epsilon\mathbf{E} = \epsilon_0\epsilon_r\mathbf{E}, \tag{2.5}$$

$$\mathbf{B} = \mu\mathbf{H} = \mu_0\mu_r\mathbf{H}, \tag{2.6}$$

$$\mathbf{J} = \sigma_c\mathbf{E}, \tag{2.7}$$

Where ϵ_0, μ_0 are the permittivity and the permeability of the free space ($\epsilon_0 \simeq 8.854 \times 10^{-12}\, F/m, \mu_0 \simeq 1.25 \times 10^{-6}\, H/m$), and $\sqrt{\epsilon_0\mu_0} = 1/c$, where c is the speed of light and equals approximately $3 \times 10^8\, m/s$). ϵ_r, μ_r are the relative permittivity and permeability for the medium. It should be noted that we consider the medium to be LHI in this thesis.

2.2 Electromagnetic Boundary Conditions

In general, for two media with different ϵ, μ, general conditions should satisfy [33]

$$(\mathbf{E}_2 - \mathbf{E}_1) \times \hat{\mathbf{n}} = \mathbf{M}_s, \tag{2.8}$$

$$\hat{\mathbf{n}} \times (\mathbf{H}_2 - \mathbf{H}_1) = \mathbf{J}_s, \tag{2.9}$$

$$\hat{\mathbf{n}} \cdot (\mathbf{D}_2 - \mathbf{D}_1) = q_e, \tag{2.10}$$

$$\hat{\mathbf{n}} \cdot (\mathbf{B}_2 - \mathbf{B}_1) = q_m, \tag{2.11}$$

Where $\hat{\mathbf{n}}$ is the normal vector on the interface pointing from region 2 to region 1, E_1, E_2 are the electric field intensity inside the first and second medium respectively, also, H_1, H_2 are the magnetic field intensity inside the first and second medium respectively, q_e, q_m are the electric and magnetic charges, $\mathbf{J}_s$ is the electric surface current density and M_s is the magnetic current density. If one of the two regions is Perfect Electric Conductor (PEC) and the other is dielectric, the boundary conditions become [33]

$$\mathbf{E}_2 \times \hat{\mathbf{n}} = 0, \tag{2.12}$$

$$\mathbf{H}_2 \times \hat{\mathbf{n}} = \mathbf{J}_s, \tag{2.13}$$

$$\hat{\mathbf{n}} \cdot \mathbf{D}_2 = 0, \tag{2.14}$$

$$\hat{\mathbf{n}} \cdot \mathbf{B}_2 = 0, \tag{2.15}$$

If PEC is replaced by perfect magnetic conductor (PMC), the boundary conditions become

$$\hat{\mathbf{n}} \times \mathbf{E}_2 = \mathbf{M}_s, \tag{2.16}$$

$$\hat{\mathbf{n}} \times \mathbf{H}_2 = 0, \tag{2.17}$$

$$\hat{\mathbf{n}} \cdot \mathbf{D}_2 = 0, \tag{2.18}$$

$$\hat{\mathbf{n}} \cdot \mathbf{B}_2 = q_m, \tag{2.19}$$

From these equations, we can describe the problem of the scattering of the electromagnetic wave from one or more scatterers. We can divide the problem into two parts: the propagation of the wave inside LHI medium, and the propagation of the wave in the interface between the objects.

2.3 Wave propagation and plan waves

Solving Maxwell's equations lead to the equation of propagating wave, which describes the electric field and magnetic field of the propagating wave everywhere. In scattering problems, an incident wave hits an object, then the wave scattered, so we can suppose this object as a radiator, and the scattered wave is a propagating wave. Consider an LHI medium, from the four Maxwell equations and some vector properties, the electric field and magnetic field should satisfy the following propagation equations [1]

$$\boldsymbol{\nabla}^2\mathbf{E} - \epsilon\mu\frac{\partial^2}{\partial t^2}\mathbf{E} = \frac{1}{\epsilon}\boldsymbol{\nabla}_\rho + \mu\frac{\partial}{\partial t}\mathbf{J}, \tag{2.20}$$

$$\boldsymbol{\nabla}^2\mathbf{H} - \epsilon\mu\frac{\partial^2}{\partial t^2}\mathbf{H} = -\boldsymbol{\nabla} \times \mathbf{J}, \tag{2.21}$$

Where equation (2.20) represents the electric field equation, in the same way, equation (2.21) represents the magnetic field equation. One of the

significant cases is the case of PEC. In this case, there is no charges in the propagating medium, so ($\rho = 0$ and $\mathbf{J} = \sigma_c \mathbf{E}$). Using equation (2.7), the equations of propagation become [1]

$$\boldsymbol{\nabla}^2 \mathbf{E} - \epsilon\mu \frac{\partial^2}{\partial t^2}\mathbf{E} - \mu\sigma_c \frac{\partial}{\partial t}\mathbf{E} = 0, \tag{2.22}$$

$$\boldsymbol{\nabla}^2 \mathbf{H} - \epsilon\mu \frac{\partial^2}{\partial t^2}\mathbf{H} - \mu\sigma_c \frac{\partial}{\partial t}\mathbf{H} = 0, \tag{2.23}$$

Other important case is the case of Perfect Dielectric Medium (PDM), where ($\rho = 0$ and $\mathbf{J} = 0$), the equations of propagation become [1]

$$\boldsymbol{\nabla}^2 \mathbf{E} - \epsilon\mu \frac{\partial^2}{\partial t^2}\mathbf{E} = 0, \tag{2.24}$$

$$\boldsymbol{\nabla}^2 \mathbf{H} - \epsilon\mu \frac{\partial^2}{\partial t^2}\mathbf{H} = 0, \tag{2.25}$$

A particular solution of the equations of propagation for equation 2.24 is called the Monochromatic progressive plane wave and is represented as

$$\Psi(\mathbf{R}, t) = \Re(\mathbf{E}(\mathbf{R}, t)) = \Re(\mathbf{E}_0 e^{\pm i(\omega t - \mathbf{k}\cdot\mathbf{R} - \phi)} = \Re(\mathbf{E}(\mathbf{R}) e^{\pm i\omega t}), \tag{2.26}$$

where

$$\mathbf{k} = \sqrt{\epsilon\mu\omega}\hat{\mathbf{k}} = \frac{2\pi}{\lambda}\hat{\mathbf{k}}, \tag{2.27}$$

Where $\Re(\mathbf{v})$ takes only the real part of the vector $\mathbf{v}$, ϕ is a constant phase term, $\mathbf{k}$ is the wave number, λ is the wave length, $\hat{\mathbf{k}}$ is a unit vector that gives the direction of the propagation of the wave. The sign $\pm$ refers to

the direction of the propagating wave. In this thesis, we would use the positive sign to refer to the propagating wave, and the vector $e^{\pm i(\omega t - \mathbf{k})}$ will be applied but we will remove it from the equations.

If we substitute $\boldsymbol{\nabla} \times \mathbf{H}$ from equation (2.2), then apply the expression of the Monochromatic progressive plane wave to the equation of the propagation, the derivative with respect to the time is reduced to multiplication by the term $i\omega$, then the equation of the propagation is called Helmholtz equation, in the case of ($\rho = 0$ and $\mathbf{J} \neq 0$) it is expressed by

$$-(\boldsymbol{\nabla} \times \boldsymbol{\nabla} \times k^2 \mathbf{E}) = (\boldsymbol{\nabla}^2 + k^2)\mathbf{E} = -i\omega\mu\mathbf{J}, \tag{2.28}$$

and for the case of ($\rho = 0$ and $\mathbf{J} = 0$), the equation becomes

$$-(\boldsymbol{\nabla} \times \boldsymbol{\nabla} \times k^2 \mathbf{E}) = (\boldsymbol{\nabla}^2 + k^2)\mathbf{E} = 0, \tag{2.29}$$

Note that if we write one of the three components of the $\mathbf{E}$ field, then it checks the scalar Helmholtz equation:

$$(\Delta + k^2)\Psi = 0, \tag{2.30}$$

Where Δ is the "Laplacian"operator.

its noticed that both $\mathbf{E}, \mathbf{H}$ are orthogonal to the direction of the propagation of the wave. The electric fields and magnetic field are related by the relation

$$\eta_0 = \frac{\|\mathbf{E}\|}{\|\mathbf{H}\|} = \sqrt{\frac{\mu_0}{\epsilon_0}}, \tag{2.31}$$

Where η_0 is the impedance of the free space and called the intrinsic impedance ($\eta_0 = 120\pi\ \Omega$).

2.4 Green's Function

Green function is the elementary solution of a linear differential equation with constant coefficients, or a linear partial equation with constant coefficients. Each component of the $\mathbf{E}$ field satisfies the scalar propagation equation where the integro-differential operator $(\Delta + k^2)$. The Green's function associated with this operator is checked by [35]

$$(\Delta k^2)\mathbf{G}(\mathbf{R}, \mathbf{R}') = \delta(\mathbf{R}, \mathbf{R}'), \tag{2.32}$$

Where $\mathbf{R}, \mathbf{R}'$ are the source point and the observation point respectively, the δ is the impulse function. The solution of equation (2.32) is given by [35]

$$\mathbf{G}(\mathbf{R}, \mathbf{R}') = \frac{e^{ik\left\|\mathbf{R}-\mathbf{R}'\right\|}}{4\pi\left\|\mathbf{R}-\mathbf{R}'\right\|}. \tag{2.33}$$

To obtain the integral representations, it is necessary to transform an volume integral to a surface integral. This is done by [35]

$$\begin{aligned}\int\int\int_V [\mathbf{Q}\cdot(\boldsymbol{\nabla}\times\boldsymbol{\nabla}\times\mathbf{P}) - \mathbf{P}\cdot(\boldsymbol{\nabla}\times\boldsymbol{\nabla}\times\mathbf{Q})]\cdot dv = \\ \int\int_S [\mathbf{P}\times(\boldsymbol{\nabla}\times\mathbf{Q}) - \mathbf{Q}\times(\boldsymbol{\nabla}\times\mathbf{P})]\cdot\hat{\mathbf{n}}\cdot ds,\end{aligned} \tag{2.34}$$

where S is a surface surrounding a volume $\mathbf{V}$ and $\hat{\mathbf{n}}$ is the normal to the surface $\mathbf{S}$ pointing outwards of the volume V. $\mathbf{P}$ and $\mathbf{Q}$ are two vector

functions of the point (also called vector field).

2.5 Huygen's Principle and Extinction Theorem

Huygens principle is based on the fact that every point of a wave is itself a radiation source of a wave. By this principle, a source of radiation can be replaced by a set of currents sources. These currents are placed on a surface closed arbitrary encompassing the original source. This theorem allows us to describe generally the radiation of a distribution of currents on a surface, or to obtain a surface integral equation of the currents induced on an object excited by an incident field. Consider the scenario shown in Figure 2.1.

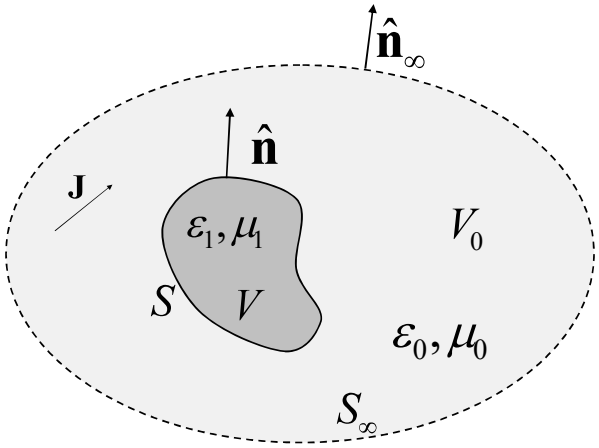

Figure 2.1: The domain Ω_0 is bounded by the contour $C_{0,\infty}$ and the surface S whereas Ω_1 is bounded by the contour $C_{1,\infty}$ and the surface S.

In Figure 2.1, the first medium which has $(\epsilon_0, \mu_0, \Omega_0)$ of volume V_0 bounded with the surface S_∞, the other medium which has $(\epsilon_1, \mu_1, \Omega_1)$ also has volume V and bounded by surface S, the source is in $\mathbf{J}$ and $\hat{\mathbf{n}}$ is the normal to the surface and always points to medium 1 (Ω_0). Applying

equation (3.2) to the volume V_0 and using Maxwell equations we have [35]

$$\begin{cases} \mathbf{E}(\mathbf{R}'), & \text{if} \quad \mathbf{R}' \in \mathrm{V}_0 \\ 0, & \text{otherwise} \end{cases} = \mathbf{E}_i(\mathbf{R}') + \int\int_S [\mathbf{G}(\mathbf{R},\mathbf{R}')i\omega\mu(\hat{\mathbf{n}}(\mathbf{R}) \times \mathbf{H}(\mathbf{R})) + (\hat{\mathbf{n}}(\mathbf{R}) \times \mathbf{E}(\mathbf{R})) \times \boldsymbol{\nabla}\mathbf{G}(\mathbf{R},\mathbf{R}') + (\hat{\mathbf{n}}(\mathbf{R}) \cdot \mathbf{E}(\mathbf{R}))\boldsymbol{\nabla}\mathbf{G}(\mathbf{R},\mathbf{R}')] \cdot ds. \tag{2.35}$$

Where $\mathbf{E}_i$ is the incident electric field, when $\mathbf{R}'$ not belong V_0 the equation (2.35) becomes [35] :

$$\mathbf{E}_i(\mathbf{R}') = -\int\int_S [\mathbf{G}(\mathbf{R},\mathbf{R}')i\omega\mu\hat{\mathbf{n}}(\mathbf{R}') \times \mathbf{H}(\mathbf{R}) + (\hat{\mathbf{n}}(\mathbf{R}) \times \mathbf{E}(\mathbf{R})) \times \boldsymbol{\nabla}\mathbf{G}(\mathbf{R},\mathbf{R}') + (\hat{\mathbf{n}}(\mathbf{R}) \cdot \mathbf{E}(\mathbf{R}))\boldsymbol{\nabla}\mathbf{G}(\mathbf{R},\mathbf{R}')] \cdot ds. \tag{2.36}$$

This equation is known as the extinction vector theorem and imposes the cancellation of the total field inside the object of volume V,the incident field being compensated for by the contribution of the surface fields. By defining the total field $\mathbf{E}$ as the sum of the incident field and the scattered field, the scattered field is expressed by [35]

$$\mathbf{E}_s(\mathbf{R}') = -\int\int_S [\mathbf{G}(\mathbf{R},\mathbf{R}')i\omega\mu\hat{\mathbf{n}}(\mathbf{R}) \times \mathbf{E}(\mathbf{R}) \times \boldsymbol{\nabla}\mathbf{G}(\mathbf{R},\mathbf{R}') + (\hat{\mathbf{n}}(\mathbf{R}) \cdot \mathbf{E}(\mathbf{R}))\boldsymbol{\nabla}\mathbf{G}(\mathbf{R},\mathbf{R}') \cdot ds. \tag{2.37}$$

Where $\mathbf{E}_s$ is the scattered electric field, this equation is known as the Huygens principle and allows the propagation of surface fields outside volume V, forming the total field after summation with the incident field.

2.6 Spherical Coordinates

For a monochromatic progressive plane wave introduced before, the electric field can be expressed in the Cartesian coordinate system by [35]

$$\mathbf{E}(\mathbf{R}) = \mathbf{E}_0 e^{i\mathbf{k}\cdot\mathbf{R}} = \begin{bmatrix} \mathbf{E}_{0x} \\ \mathbf{E}_{0y} \\ \mathbf{E}_{0z} \end{bmatrix} \cdot e^{i\mathbf{k}\cdot\mathbf{R}} \tag{2.38}$$

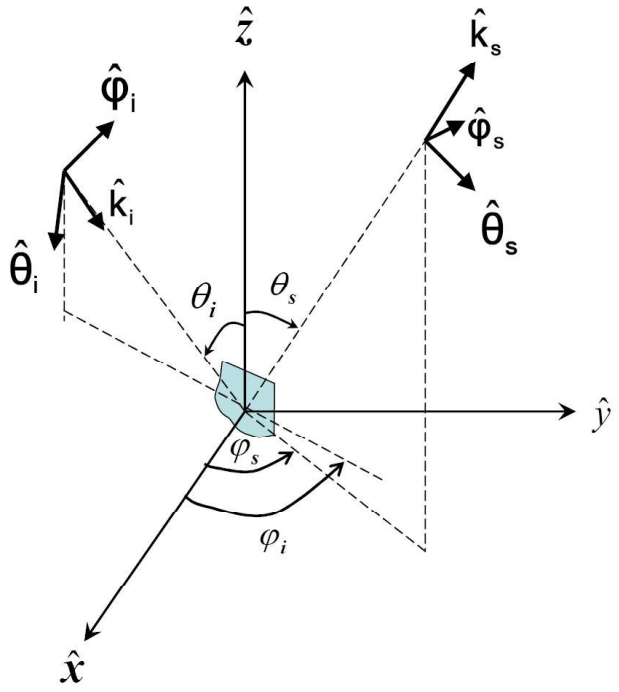

Figure 2.2: Illustration of spherical coordinates polarization bases used in transmission and reception.

where $\mathbf{E}_0$ is the magnitude of the electric field, $\mathbf{E}_{0x}, \mathbf{E}_{0y}, \mathbf{E}_{0z}$ are the magnitude if the i=electric field in the $x, yandz$ directions. Sometimes it is more efficient to describe the electric field in other coordinates like spherical coordinates. The spherical coordinates describe with the unit vectors $(\hat{\mathbf{k}}, \hat{\boldsymbol{\theta}}, \hat{\boldsymbol{\phi}})$ as shown in Figure 2.2. The incident field is described by $(\hat{\mathbf{k}}_i, \hat{\boldsymbol{\theta}}_{\boldsymbol{i}}, \hat{\boldsymbol{\phi}}_{\boldsymbol{i}})$ and the scattered field is noted by $(\hat{\mathbf{k}}_s, \hat{\boldsymbol{\theta}}_{\boldsymbol{s}}, \hat{\boldsymbol{\phi}}_{\boldsymbol{s}})$. Since electric fields are orthogonal to the propagation directions, we get:

$$\mathbf{E}_i(\mathbf{R}) = \mathbf{E}_{0i} e^{i\mathbf{ki}\cdot\mathbf{R}} = \begin{bmatrix} 0 \\ \mathbf{E}_{0i}^{\theta} \\ \mathbf{E}_{0i}^{\phi} \end{bmatrix} \cdot e^{i\mathbf{k}_i\cdot\mathbf{R}} \tag{2.39}$$

$$\mathbf{E}_s(\mathbf{R}) = \mathbf{E}_{0s} e^{i\mathbf{ks}\cdot\mathbf{R}} = \begin{bmatrix} 0 \\ \mathbf{E}_{0s}^{\theta} \\ \mathbf{E}_{0s}^{\phi} \end{bmatrix} \cdot e^{i\mathbf{k}_s\cdot\mathbf{R}} \tag{2.40}$$

In this thesis, we might convert between the Cartesian coordinates and the spherical coordinates and vise versa, the conversion can be done using the following spherical rotation matrices $\bar{\mathbf{R}}_i$ and $\bar{\mathbf{R}}_s$ [35]

$$\bar{\mathbf{R}}_i(\theta_i, \phi_i) = \begin{bmatrix} \sin\theta_i \cos\phi_i & -\cos\theta_i \cos\phi_i & -\sin\phi_i \\ \sin\theta_i \sin\phi_i & -\cos\theta_i \sin\phi_i & \cos\phi_i \\ -\cos\theta_i & -\sin\theta_i & 0 \end{bmatrix} \tag{2.41}$$

$$\bar{\mathbf{R}}_s(\theta_s, \phi_s) = \begin{bmatrix} \sin\theta_s \cos\phi_s & \cos\theta_s \cos\phi_s & -\sin\phi_s \\ \sin\theta_s \sin\phi_s & \cos\theta_s \sin\phi_s & \cos\phi_s \\ \cos\theta_s & -\sin\theta_s & 0 \end{bmatrix} \tag{2.42}$$

The vectors of the spherical bases are defined by [35]:

$$\begin{bmatrix} \hat{\mathbf{k}}_i \\ \hat{\boldsymbol{\theta}}_i \\ \hat{\boldsymbol{\phi}}_i \end{bmatrix} = \bar{\mathbf{R}}_i(\theta_i, \phi_i)^T \begin{bmatrix} \hat{\mathbf{x}} \\ \hat{\mathbf{y}} \\ \hat{\mathbf{z}} \end{bmatrix} \tag{2.43}$$

and

$$\begin{bmatrix} \hat{\mathbf{k}}_s \\ \hat{\boldsymbol{\theta}}_s \\ \hat{\boldsymbol{\phi}}_s \end{bmatrix} = \bar{\mathbf{R}}_s(\theta_s, \phi_s)^T \begin{bmatrix} \hat{\mathbf{x}} \\ \hat{\mathbf{y}} \\ \hat{\mathbf{z}} \end{bmatrix} \tag{2.44}$$

where T is the Transpose.

2.7 Diffraction Matrix

The incident electric field $\mathbf{E}_i$ and the scattered electric field $\mathbf{E}_s$from an object can be connected by diffraction matrix (diffusion matrix). We decompose the $\mathbf{E}_i, \mathbf{E}_s$ into two orthogonal components depending on its polarization, the component of the incident electric field in the direction of θ ($\mathbf{E}_i^{\theta}$), the component of the incident electric field in the direction of ϕ ($\mathbf{E}_i^{\phi}$),the component of the scattered electric field in the direction of

θ ($\mathbf{E}_s^{\theta}$), the component of the incident electric field in the direction of ϕ ($\mathbf{E}_s^{\phi}$), we obtain the relation:

$$\begin{bmatrix} \mathbf{E}_s^{\theta} \\ \mathbf{E}_s^{\phi} \end{bmatrix} = \bar{\mathbf{S}} \begin{bmatrix} \mathbf{E}_i^{\theta} \\ \mathbf{E}_i^{\phi} \end{bmatrix} \tag{2.45}$$

where $\bar{\mathbf{S}}$ is the scattering matrix and defined as

$$\bar{\mathbf{S}} = \begin{bmatrix} \mathbf{S}_{\theta\theta} & \mathbf{S}_{\theta\phi} \\ \mathbf{S}_{\phi\theta} & \mathbf{S}_{\phi\phi} \end{bmatrix} \tag{2.46}$$

Where $\mathbf{S}_{\theta\theta}$ is the scattering parameter when the incident electric field in the direction of θ, and the scattered field in the direction of θ, the other elements of $\bar{\mathbf{S}}$ are defined. The knowledge of the four terms of the diffraction matrix is sufficient to define the response of an object subjected to a completely arbitrary polarization state wave. The scattering matrix components are necessary to calculate the RCS.

2.8 Radar Cross Section (RCS)

Depending on the location of the observation point with respect to the source point, we can divide it into two regions, the far field region, that is the region where the measuring point is very far from the source. In deeper look, Figure 2.3 shows two cases.

From Figure 2.3, the near field is defined when the source point and

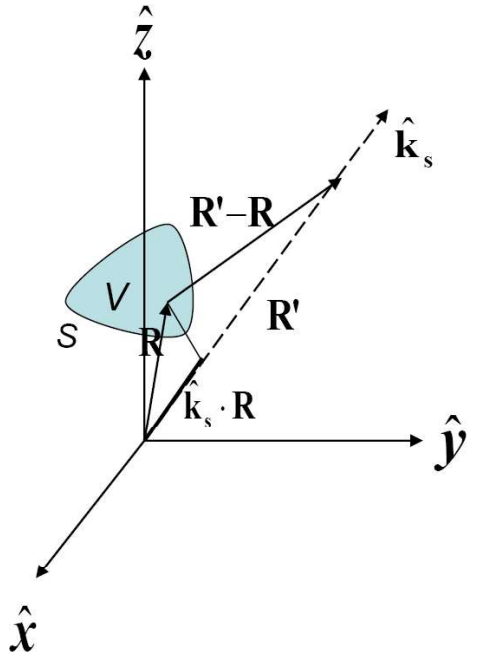

Figure 2.3: Near and Far field geometry.

the object are near ($\mathbf{R} = \left\|\mathbf{R} - \mathbf{R}'\right\|$) can not be ignored), but in the second case, where the observation point is very far from the source, an approximation can be done ($\mathbf{R} = \mathbf{R}'$). Depending on this approximation, the green function can be approximated as

$$\mathbf{G}(\mathbf{R}, \mathbf{R}') = \frac{e^{ik\left\|\mathbf{R}-\mathbf{R}'\right\|}}{4\pi\left\|\mathbf{R}-\mathbf{R}'\right\|} \approx \frac{e^{ik\mathbf{R}'}}{4\pi R'} e^{-ik\hat{\mathbf{k}}_s \cdot \mathbf{R}} \tag{2.47}$$

One of the applications on the far field region is the RCS. RCS is commonly used to characterise the reflected wave from an object. It is denoted by the ratio of the power density scattered from an object to the power density of the incident wave at the same object. The reflected power gives a good indication about the capacity of the object. RCS depends on several variables like the carrier frequency of the incident plane wave, polarization state on the transmission and reception, the

geometric of the object, the properties of the object $(\mu, \epsilon, \sigma_c)$, and the angle between the incident wave and the object. For the plane on the vacuum, the average power densities are:

$$\left\|\langle \mathbf{\Pi}_i \rangle_t\right\| = \frac{\left\|\mathbf{E}_i\right\|^2}{2\eta_0}, \tag{2.48}$$

$$\left\|\langle \mathbf{\Pi}_s \rangle_t\right\| = \frac{\left\|\mathbf{E}_s\right\|^2}{2\eta_0}, \tag{2.49}$$

where $\left\|\langle \mathbf{\Pi}_i \rangle_t\right\|, \left\|\langle \mathbf{\Pi}_s \rangle_t\right\|$ are the time average of the pointing vector for the incident wave and the scattered wave respectively.

Keep in mined that the total incident power is equal to the sum of the transmitted power through the object and the reflected power from it, as

$$P_i = P_t + P_s, \tag{2.50}$$

Depends on equation (2.48) and equation (2.49), the RCS of an object in the far field is expressed as follow

$$\sigma(\mathbf{k}_i, \mathbf{k}_s) = 4\pi R'^2 \frac{\left\|\langle \mathbf{\Pi}_s \rangle_t\right\|}{\left\|\langle \mathbf{\Pi}_i \rangle_t\right\|} = 4\pi R'^2 \frac{\left\|\mathbf{E}_s\right\|^2}{\left\|\mathbf{E}_i\right\|^2}, \tag{2.51}$$

The previous definition of RCS does not take in account the polarization state of the incident wave. If we consider the projection of the incident wave polarization in the spherical coordinates, the RCS matrix

is deduced from the diffraction matrix by the following relation

$$\bar{\boldsymbol{\sigma}} = \begin{bmatrix} \sigma_{\theta\theta} & \sigma_{\theta\phi} \\ \sigma_{\phi\theta} & \sigma_{\phi\phi} \end{bmatrix} = \lim_{R' \to \infty} 4\pi R'^2 \begin{bmatrix} \|S_{\theta\theta}\|^2 & \left\|S_{\theta\phi}\right\|^2 \\ \left\|S_{\phi\theta}\right\|^2 & \left\|S_{\phi\phi}\right\|^2 \end{bmatrix} \tag{2.52}$$

Where $\sigma_{\theta\theta}$ is the RCS for the the θ component of the incident electric field with the θ component of the scattered electric field, the other elements of $\bar{\boldsymbol{\sigma}}$ are defined in the same way.

This diffraction matrix is called the polarimetric signature. The knowledge of all elements of the diffraction matrix gives a good indication about the response of the object subjected to a completely arbitrary polarization state wave.

2.9 Conclusion

In this chapter, we discussed Maxwell's equations and the boundary conditions, from that, we are able to know the behaviour of the wave in the medium and the interface between two media. Also, the green's functions as a solution for the linear differential equation were defined.

We will use the definitions that introduced in this chapter in the following chapters to compute the scattering field for several scenarios, and compute the RCS for each scenario using MoM and other methods.

Chapter 3

Electromagnetic Scattering From Single Scatterer

The method of moment (MoM) is one of the popular methods to compute the scattering field. In this chapter, we introduce the Integral Equations (IE), then we explain in details the method of moment and how to use it. After that, MoM is applied on a thin wire and a rectangular plate to calculate the charge density, then the MoM is applied for scattering problems from a square plate and the rough surface. For each case, the simulation results are displayed and discussed.

3.1 Integral Equations

Consider the problem of the form

$$L(f) = g, \tag{3.1}$$

where L is any linear operator, such as an Integral, deferential or integrodifferential operator, f is unknown and g is known. Solving this kind of problems where the unknown is inside an operator is not easy. One of the efficient methods to find f is by expanding the unknown by a set

of known basis functions

$$f = \sum_{n=1}^{N} a_n f_n, \tag{3.2}$$

Where N is the number of weighting bases functions, a_n are unknowns weighting coefficients.

In this case, the totally unknown f is represented by a set of known bases functions. Now, solving this problem becomes easier since we substitute equation (3.2) in equation (3.1) to have

$$\sum_{n=1}^{N} a_n L(f_n) \cong g, \tag{3.3}$$

The error of using this expansion is calculated by

$$R = g - \sum_{n=1}^{N} a_n L(f_n), \tag{3.4}$$

The value of R depends on the bases function used. The choice of these bases functions depends mainly on the problem and the behaviour of the unknown functions.

3.2 Method of Moment (MoM)

MoM is a well-known method to solve scattering integral equations. As illustrated in the previous chapter. MoM solves the Integral Equations (IE) by converting it to a linear system in the form of $\bar{\mathbf{Z}}\mathbf{X} = \mathbf{b}$, where $\mathbf{X}$

is the vector of unknowns, $\bar{\mathbf{Z}}$ is called impedance matrix and $\mathbf{b}$ is vector of knowns. In this form, it becomes easy to find $\mathbf{X} = \bar{\mathbf{Z}}^{-1}\mathbf{b}$, notice that solving this equation depends mainly on $\bar{\mathbf{Z}}$. As the dimension of $\bar{\mathbf{Z}}$ matrix increases, the computation time and memory requirements rapidly increase too, this is the main limitation of MoM.

To use MoM we defined the inner product between basis functions $f_n(\mathbf{R}')$ and the testing or weighting functions $f_m(\mathbf{R})$ as [36]

$$< f_m, f_n >= \int_{f_m} f_m(\mathbf{R}) \cdot \int_{f_n} f_n(\mathbf{R}') \cdot dR'dR, \tag{3.5}$$

Where the integral is a line, surface or volume, depends on the basis functions. Applying equation (3.5) on equation (3.4) we have

$$\sum_{n=1}^{N} a_n < f_m, L(f_n) >=< f_m, g >, \tag{3.6}$$

We can convert this form to an $N \times N$ matrix equation in the form $\bar{\mathbf{Z}}\mathbf{X} = \mathbf{b}$. The elements of $\bar{\mathbf{Z}}$ are computed by

$$\bar{\mathbf{Z}}_{mn} =< f_m, L(f_n) >, \tag{3.7}$$

In the scattering problems, $\bar{\mathbf{Z}}$ is defined as the impedance matrix to be calculated, $\mathbf{X}$ is the set of unknowns, which are the surface current and $\mathbf{b}$ is the set of knowns, which are the voltage of the incident wave.

Solving this system leads to find the distribution of the current on the illuminated surface.

To have a good illustration of MoM we will apply it in details on electrostatic problems (thin wire and plate), then we would use it on scattering problems.

3.2.1 Charged thin wire

To begin, consider a very thin wire of radius d and length L, located along the x axis. If the length of the wire is very long compared with its radius (L>> d) as shown in Figure 3.1, then the electric potential along it is described as [37]

Figure 3.1: A thin conductive wire with length L.

$$\Phi_e(\mathbf{R}) = \int_0^L \frac{q_e(\mathbf{R}')}{4\pi\epsilon\left\|\mathbf{R}-\mathbf{R}'\right\|} \cdot dx', \tag{3.8}$$

Where $q_e(\mathbf{R}')$ is the electric charge in the observation point ($\mathbf{R}'$) and $\left\|\mathbf{R}-\mathbf{R}'\right\| = \sqrt{(x-x')^2+(y-y')^2}$ is the distance between the source point ($\mathbf{R}$) and the observation point ($\mathbf{R}'$).

If $q_e(\mathbf{R}')$ is known, the solution of this equation becomes easy, but if $q_e(\mathbf{R}')$ is unknown, equation (3.8) becomes an integral equation, so we apply MoM to solve it for $q_e(\mathbf{R}')$.

First, we divide the wire to small segments with length of Δx as shown in Figure 3.2, and we suppose that $q_e(\mathbf{R}')$ is constant along the wire, if we use rectangular basis functions, we can expand $q_e(\mathbf{R}')$ as

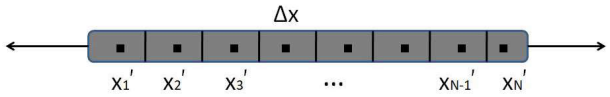

Figure 3.2: The line divided to segments of length Δx.

$$q_e(x') = \sum_{n=1}^{N} a_n f_n(x') \tag{3.9}$$

Where a_n are the unknown weighting coefficients, and $f_n(x')$ is set of the rectangular basis functions defined as [37]

$$f_n(x') = \begin{cases} 0, & if x' < (n-1)\Delta x, \\ 1, & if (n-1)\Delta x \leq x' \leq n\Delta x, \\ 0, & if x' > n\Delta x, \end{cases} \tag{3.10}$$

In order to solve this system, the value of Φ_e should be known, to simplify the derivations, we assume that $\Phi_e = 1$ V, now substituting these on equation(3.8) leads to [37]

$$1 = \int_0^L \sum_{n=1}^{N} a_n f_n(x') \frac{1}{4\pi\epsilon \left\| \mathbf{R} - \mathbf{R}' \right\|} \cdot dx, \tag{3.11}$$

we can rewrite equation (3.11) as [37]

$$1 = \frac{1}{4\pi\epsilon} \sum_{n=1}^{N} a_n \int_{(n-1)\Delta x}^{n\Delta x} \frac{1}{\left\|\mathbf{R} - \mathbf{R}'\right\|} \cdot dx', \tag{3.12}$$

In equation (3.12), the total integral is converted to a sum of sub integrals, each integration is over one pulse function. Also, to simplify the derivation, we assume the source points are located at the wire axis, while the observation points are distributed on the surface of the wire, as a result of this assumption, we can write

$$\left\|\mathbf{R} - \mathbf{R}'\right\| = \sqrt{(x - x') + d^2}, \tag{3.13}$$

depends on this result, we can rewrite equation (3.12) as

$$4\pi\epsilon = a_1 \int_{0}^{\Delta x} \frac{1}{\sqrt{(x-x')^2 + d^2}} \cdot dx' + a_2 \int_{\Delta x}^{2\Delta x} \frac{1}{\sqrt{(x-x')^2 + d^2}} \cdot dx'$$
$$+ \cdots + a_{N-1} \int_{(N-2)\Delta x}^{(N-1)\Delta x} \frac{1}{\sqrt{(x-x')^2 + d^2}} \cdot dx' + a_N \int_{(N-1)\Delta x}^{(N)\Delta x} \frac{1}{\sqrt{(x-x')^2 + d^2}} \cdot dx',$$

In this equation, we have N unknowns, but this equation describes only one source point at location x. To solve this system, we should have N equations with N unknowns. We can do that by applying this equation to all the source points we have, and the previous equation becomes

$$4\pi\epsilon = a_1 \int_0^{\Delta x} \frac{1}{\sqrt{(x_1 - x')^2 + d^2}} \cdot dx' + a_2 \int_{\Delta x}^{2\Delta x} \frac{1}{\sqrt{(x_1 - x')^2 + d^2}} \cdot dx'$$
$$+ \cdots + a_{N-1} \int_{(N-2)\Delta x}^{(N-1)\Delta x} \frac{1}{\sqrt{(x_1 - x')^2 + d^2}} \cdot dx' + a_N \int_{(N-1)\Delta x}^{(N)\Delta x} \frac{1}{\sqrt{(x_1 - x')^2 + d^2}} \cdot dx',$$

$$4\pi\epsilon = a_1 \int_0^{\Delta x} \frac{1}{\sqrt{(x_2 - x')^2 + d^2}} \cdot dx' + a_2 \int_{\Delta x}^{2\Delta x} \frac{1}{\sqrt{(x_2 - x')^2 + d^2}} \cdot dx'$$
$$+ \cdots + a_{N-1} \int_{(N-2)\Delta x}^{(N-1)\Delta x} \frac{1}{\sqrt{(x_2 - x')^2 + a^2}} \cdot dx' + a_N \int_{(N-1)\Delta x}^{(N)\Delta x} \frac{1}{\sqrt{(x_2 - x')^2 + d^2}} \cdot dx',$$

$$\vdots$$

$$4\pi\epsilon = a_1 \int_0^{\Delta x} \frac{1}{\sqrt{(x_N - x')^2 + d^2}} \cdot dx' + a_2 \int_{\Delta x}^{2\Delta x} \frac{1}{\sqrt{(x_N - x')^2 + d^2}} \cdot dx'$$
$$+ \cdots + a_{N-1} \int_{(N-2)\Delta x}^{(N-1)\Delta x} \frac{1}{\sqrt{(x_N - x')^2 + d^2}} \cdot dx' + a_N \int_{(N-1)\Delta x}^{(N)\Delta x} \frac{1}{\sqrt{(x_N - x')^2 + d^2}} \cdot dx',$$

and this system can be presented in matrix notation in the form of

$\bar{\mathbf{Z}}\mathbf{X} = \mathbf{b}$ as following

$$\begin{bmatrix} Z_{11} & Z_{12} & Z_{13} & \cdots Z_{1N} \\ Z_{21} & Z_{22} & Z_{23} & \cdots Z_{2N} \\ \vdots & & & \\ Z_{N1} & Z_{N2} & Z_{N3} & \cdots Z_{NN} \end{bmatrix} \begin{bmatrix} a_1 \\ a_2 \\ \vdots \\ a_N \end{bmatrix} = \begin{bmatrix} b_1 \\ b_2 \\ \vdots \\ b_N \end{bmatrix} \tag{3.14}$$

comparing the previous equations, we conclude the elements of $\bar{\mathbf{Z}}$ matrix as

$$Z_{mn} = \int_{(n-1)\Delta x}^{n\Delta x} \frac{1}{\sqrt{(x_m - x')^2 + d^2}} \cdot dx' \tag{3.15}$$

and $\mathbf{b}_m = 4\pi\epsilon$, some gives simplified formula to find the elements of $\bar{\mathbf{Z}}$ as

$$Z_{mn} = log\Big[\frac{(x_b - x_m) + \sqrt{(x_b - x_m)^2 - d^2}}{(x_a - x_m) + \sqrt{(x_a - x_m)^2 - d^2}}\Big], \tag{3.16}$$

where $X_b = n\Delta x$, $X_a = (n-1)\Delta x$.

We test these equations on a wire of length 1 m, and radius of 0.001 m, $\Phi_e = 1$ v. Figures 3.3, 3.4 show the charge distribution when we use 10, 100 segments respectively. Because the wire is very thin, the charges distribute equally on the surface of the wire along its length. This result is clear in Figure 3.4, the charge is approximately the same along the wire except for the edges. On the other hand, Figure 3.3 does not give the same indication and the shown result is not accurate. The error represented in equation (3.4) can be reduced by increasing the number

of unknowns as shown in our results.

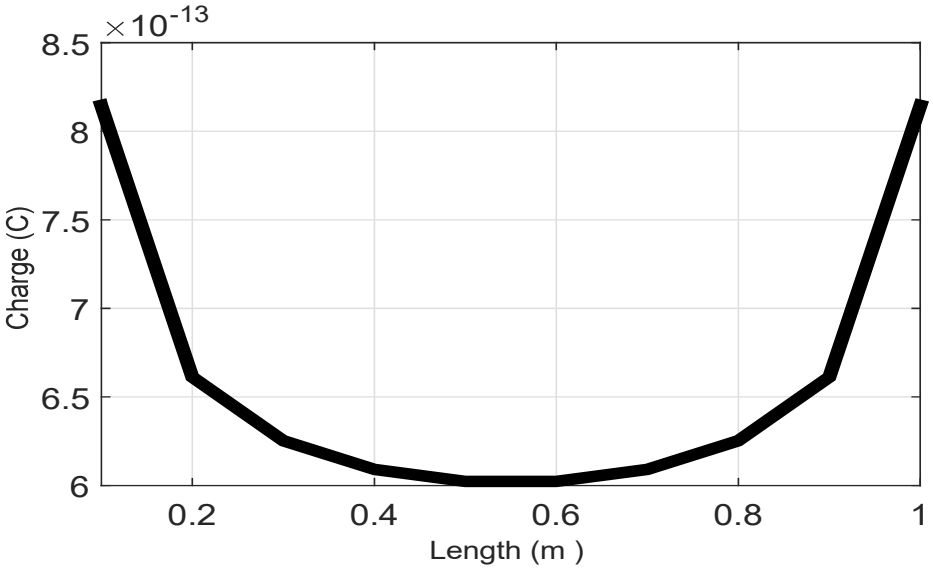

Figure 3.3: Charge distribution on a wire of length = 1 m and radius = 0.001 m when applying voltage potential of 1 V, the wire is divided into 10 segments using MoM.

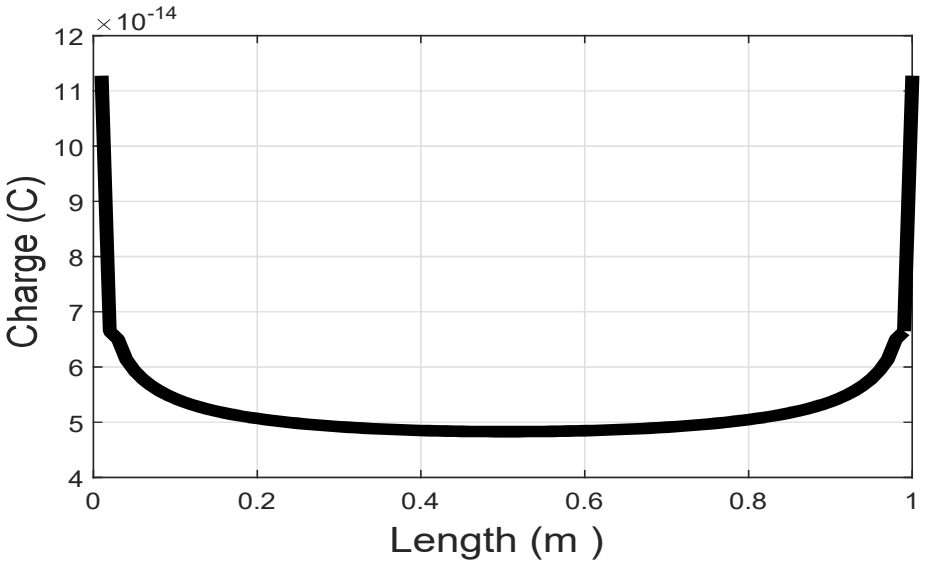

Figure 3.4: Charge distribution on a wire of length = 1 m and radius = 0.001 m when applying voltage potential of 1 V, the wire is divided into 100 segments using MoM.

3.2.2 Charged plate

Let us take thin charged conducting square plate with length L as shown in Figure 3.5.

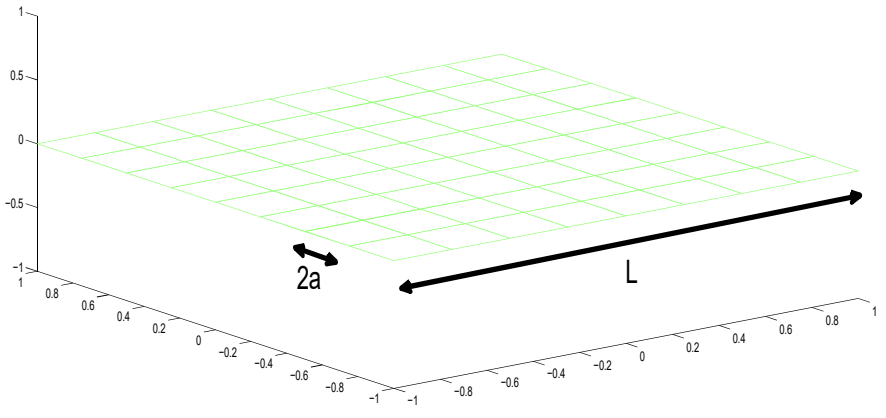

Figure 3.5: Square plate of length L discretized to small square patches each of length $2a$.

The potential on the plate is given by [37]

$$\Phi_e(\mathbf{R}) = \int_{-L/2}^{L/2}\int_{-L/2}^{L/2} \frac{q_e(x',y')}{4\pi\epsilon\left\|\mathbf{R}-\mathbf{R}'\right\|}\cdot dx'dy', \tag{3.17}$$

we suppose the potential on the plate to be 1 v, then the above equation becomes

$$4\pi\epsilon = \int_{-L/2}^{L/2}\int_{-L/2}^{L/2} \frac{q_e(x',y')}{\sqrt{(x-x')^2+(y-y')^2}}\cdot dx'dy', \tag{3.18}$$

Now, we discretize the plate to N square patches, each of length $2a$, the area of each patch is $4a^2$, and we suppose we have N observation point, each point is located at the center of the patch. However, we can convert equation (3.18) to a linear equation in the form of $\bar{\mathbf{Z}}\mathbf{X} = \mathbf{b}$, the elements of the $\bar{\mathbf{Z}}_{mn}$ matrix are described as

$$Z_{mn} = \int\int_{S_2} \frac{1}{\sqrt{(x_m - x')^2 + (y_m - y')^2}}, \tag{3.19}$$

Where S_n is the area of each square patch. In this case, the vector $\mathbf{b}$ remains the same as the case of the thin wire.

Applying equation (3.19) leads to a problem in the case when $m = n$. In other words, when the source point is itself the observation point. These points should be calculated analytically by a different equation as [37], we will use the formula [37]

$$Z_{mm} = \frac{2a}{\pi\epsilon} log(1 + \sqrt{2}) \tag{3.20}$$

Figures 3.6 and 3.7 show respectively the computed surface charge densities for 10 and 20 segments in the x, y directions. We have 121, 441 unknowns, from the figures, we notice that the surface charge density accumulates near the corners and the edge of the plate.

3.2.3 Method of Moments applied for scattering problem (Scattering from Plate)

In the previous section, we studied examples of electrostatic cases. Now, we will study the cases of wave scattering from a square plate.

Consider a thin perfectly conductor square plate is illuminated by a plane

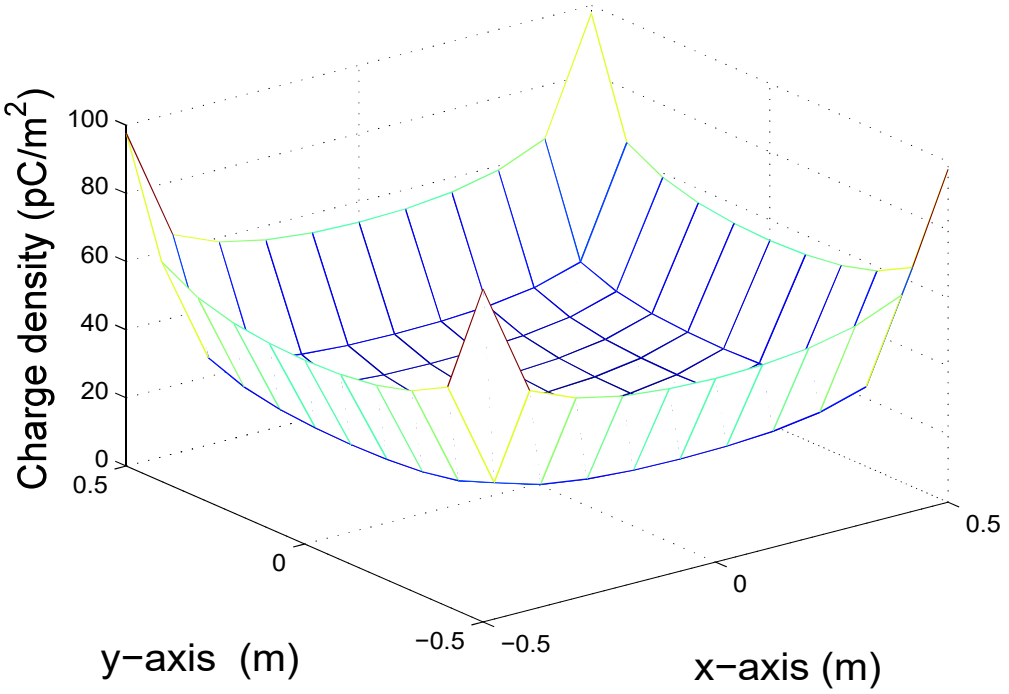

Figure 3.6: The computed surface charge density of square plate of length 1 m, with 10 segments using MoM

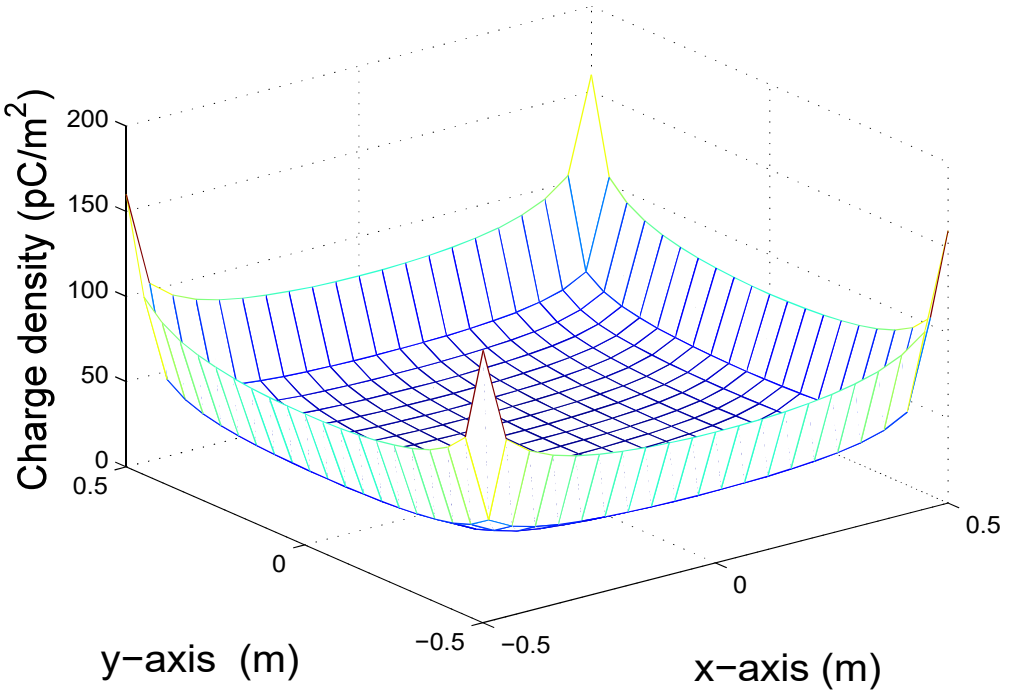

Figure 3.7: The computed surface charge density of square plate of length 1 m, with 100 segments using MoM

wave as shown in Figure 3.8. The incident wave is represented by

$$\mathbf{E}_i(\mathbf{R}) = \hat{\mathbf{e}}_i e^{i\mathbf{k}_i \cdot \mathbf{R}}, \tag{3.21}$$

and the incident magnetic field is

$$\mathbf{H}_i(\mathbf{R}) = \frac{1}{\eta_0}\hat{\mathbf{k}}_i \times \mathbf{E}_i(\mathbf{R}), \tag{3.22}$$

where $\eta_0 = \sqrt{\frac{\mu_0}{\epsilon_0}}$ is the intrinsic impedance.

The Magnetic field integral equation (MFIE) for perfectly conducting surface is [37]

$$(\frac{1}{2} + \bar{\mathbf{M}})\mathbf{J} = \hat{\mathbf{n}} \times \mathbf{H}_i, \tag{3.23}$$

where $\bar{\mathbf{M}}$ is the integro-differential operator, $\mathbf{J}$ is the surface current, $\hat{\mathbf{n}}$ is the unit vector normal to the plane, and $\mathbf{H}_i$ is the incident magnetic field. Let us defined $\mathbf{c}$ to be the surface density, $\mathbf{R}, \mathbf{R}'$ are two points on the surface (S), then

$$\bar{\mathbf{M}}\mathbf{c}(\mathbf{R}) = \hat{\mathbf{n}} \times \boldsymbol{\nabla}_{\mathbf{R}} \int_S G(\mathbf{R} - \mathbf{R}')\mathbf{c}(\mathbf{R}') \cdot ds, \tag{3.24}$$

where $\boldsymbol{\nabla}_{\mathbf{R}}$ is made up of the partial derivatives with respect to $\mathbf{R}$, the last equation can be written in the form

$$\bar{\mathbf{M}}\mathbf{c}(\mathbf{R}) = \hat{\mathbf{n}}(\mathbf{R}) \times \int_S G'(\mathbf{R})\mathbf{u} \times \mathbf{c}(\mathbf{R}') \cdot ds \tag{3.25}$$

$$= \int_S G'(R)\hat{\mathbf{n}} \times (\mathbf{u} \times \mathbf{c}(\mathbf{R}'))\Gamma' \cdot dx'dy'. \tag{3.26}$$

Where $G'(R)$ is the first derivative of the green function, $R = \left\|\mathbf{R} - \mathbf{R}'\right\|$ and $\mathbf{u} = (\mathbf{R} - \mathbf{R}')/R$. Each point is describes in the form $\mathbf{R}(x, y, z)$, then z is a function of the x and y coordinates. For the surface S, the z coordinates is $z = f(x, y)$, $z_x = \frac{\partial}{\partial x} f$ and $z_y = \frac{\partial}{\partial y} f$, Γ in the previous equation is $\Gamma = \sqrt{1 + z_x^2 + z_y^2}$, the unit vector $\hat{\mathbf{n}} = ((-z_x\hat{\mathbf{x}} - z_y\hat{\mathbf{y}} +' \hat{\mathbf{z}})/\Gamma)$. Suppose that the surface density c is tangent to the surface S, $c \cdot n = 0$, should be satisfied, and

$$c_z = z_x c_x + z_y c_y, \tag{3.27}$$

Where $c_x = \Gamma\mathbf{c} \cdot \hat{\mathbf{x}}$, $c_y = \Gamma\mathbf{c} \cdot \hat{\mathbf{y}}$ and $c_z = \Gamma\mathbf{c} \cdot \hat{\mathbf{z}}$. These relations are described by the Cartesian coordinates, they can be converted to other coordinates when necessary. The surface density c can be expressed by only c_x and c_y, since c_x and c_y are independent.

From equation (3.23), special attention should be taken in the case of $G'(R)$, the first derivative of the green function. Since it is equal $1/R^2$. To overcome this case, we associate four scaler operators $M_{xx}, M_{xy}, M_{yx}, M_{yy}$ to the $\bar{\mathbf{M}}$ operator to become

$$\begin{bmatrix} \Gamma M\mathbf{c} \cdot \mathbf{x} \\ \Gamma M\mathbf{c} \cdot \mathbf{x} \end{bmatrix} = \begin{bmatrix} M_{xx} & M_{xy} \\ M_{yx} & M_{yy} \end{bmatrix} \begin{bmatrix} c_x \\ c_y \end{bmatrix} \tag{3.28}$$

Substitute these results in equation (refn20), it becomes

$$\begin{bmatrix} M_{xx} & M_{xy} \\ M_{yx} & M_{yx} \end{bmatrix} \begin{bmatrix} c_x \\ c_y \end{bmatrix} = \int_S G'(R) \begin{bmatrix} z'_x u_x + z_y u_y - u_z & (z'_y - z_y)u_x \\ (z'_x - z_x)u_y & z_x u_x + z'_y uy - u_z \end{bmatrix} \begin{bmatrix} c_x \\ c_y \end{bmatrix} \cdot dx' dy \tag{3.29}$$

In order to calculate the scattered field and the radar cross section for the plate using MoM, we discretize the plat to square segments, each segment has dimension of $x \in [x_k - \Delta x/2; x_k + \Delta x/2]$ and $y \in [y_k - \Delta y/2, y_k + \Delta y/2]$. We should take in the account that the surface satisfies the cartesian equation $z = f(x, y)$. We will use the pulse function as the basis functions located at the center of each segment. The constant values on the cell(N) of the two functions c_x, c_y are associated with the current c constitute two vectors with N complex elements. We denote by c_x the component vector c_{xj} equal to c_x on the surface (S_j) and c_y the component vector c_{yj} equal to c_y on S_j. Now, we consider the unknowns J_x and J_y for the surface electric current and J_i^x, J_i^y are the incident electric field tangent to the surface

$$J_{xj} = \mathbf{\Gamma}_j \hat{\mathbf{x}} \cdot (\hat{\mathbf{n}} \times \mathbf{H}(\mathbf{R}_j)), J_i^{xj} = \Gamma_j \hat{\mathbf{x}} \cdot (\hat{\mathbf{n}} \times \mathbf{H}_i(\mathbf{R}_j)), \tag{3.30}$$

$$J_{yj} = \mathbf{\Gamma}_j \hat{\mathbf{y}} \cdot (\hat{\mathbf{n}} \times \mathbf{H}(\mathbf{R}_j)), J_i^{yj} = \Gamma_j \hat{\mathbf{y}} \cdot (\hat{\mathbf{n}} \times \mathbf{H}_i(\mathbf{R}_j)). \tag{3.31}$$

We tested the model of a square plate located at the plane $(\hat{x}, O, \hat{y})$ for normal incidence. Figure 3.8 shows the plate with the incident and

reflected fields, where (θ_i, ϕ_i) are the angles of the incident field, (θ_s, ϕ_s) are the angles of the scattered field, $\hat{\mathbf{k}}_i, \hat{\mathbf{k}}_s$ represent the direction of the incident and scattered fields respectively, and the normal to the surface is pointing to the $\hat{z}$ axis.

Figure 3.9 shows a comparison of the RCS calculated by the proposed MoM and the one obtained from EM simulator FEKO MLFMM(Multi Level Fast Multi pole Method)[38]. The plate has dimension of $10\lambda_0 \times 10\lambda_0$, the angle of the incident wave is $\theta_i = 0, \phi_i = 0$. Figure 3.10 shows the current distribution on the plate after excited by a plane wave, and the RCS. From the figure, it is clearly shown that the current distributes mostly at the edges of the plate. the results shows good agreements especially at the incident angles, while the RCS at the edges show some differences.

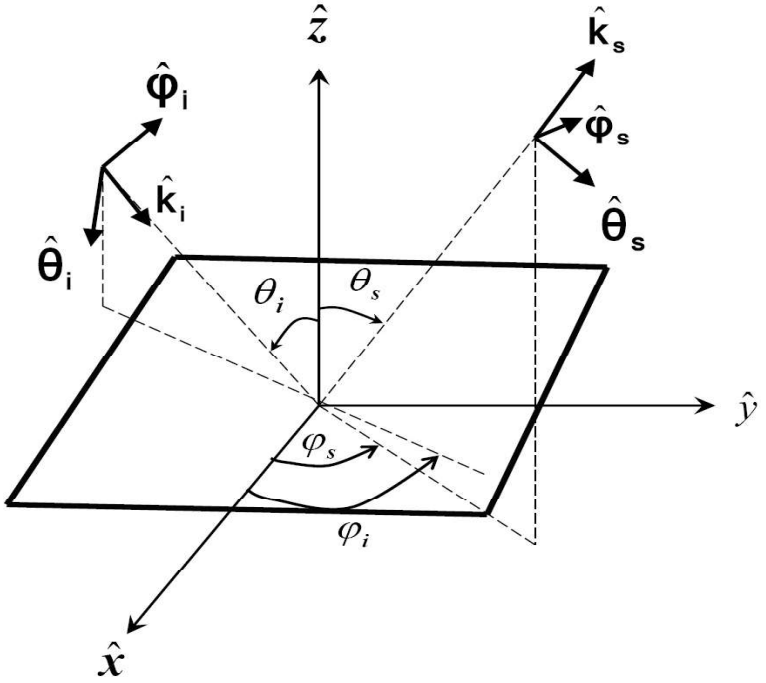

Figure 3.8: The geometry of the problem: the excitation of square plat by plane wave.

More over, we tested the RCS for vertical polarization for the same case,

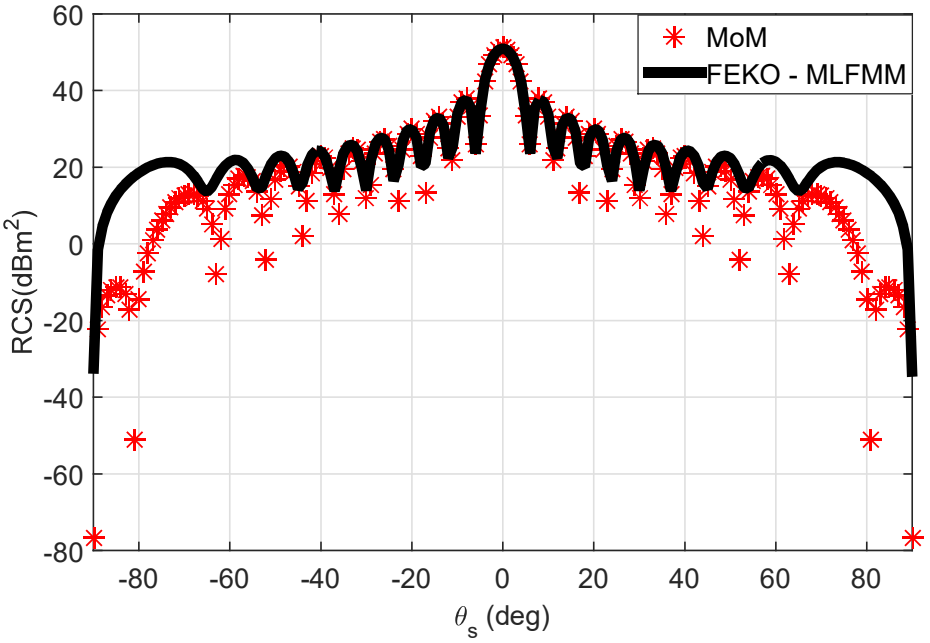

Figure 3.9: Comparison of the RCS from MoM and the results from FEKO for horizontal polarization, the square plate has dimensions $10\lambda_0 \times 10\lambda_0$, $\Delta x = \Delta y = \lambda_0/8$ $\theta_i = 0^o$, $\phi_i = 0^o$.

and compared it with FEKO as shown in Figure 3.11, the results also shows a good agreements for most scattering angles and some differences at the edges.

3.2.4 Rough surface

In the previous section, we discussed the scattering from square plate, other important case is the rough surface, as shown in Figure 3.12. To calculate the scattered field from rough surface using MoM, we mesh the surface to small segments, each segment of the surface S_j is approximated by its plane tangent to the point $\mathbf{R}_j$, also, the normal at every point on the surface S_j is the normal $(\mathbf{n}_j)$ at the point $(\mathbf{R}_j)$. In this case, the first derivative z'_x, z'_y are constant and equal to z_{xj}, z_{yj} at each point R_i of the

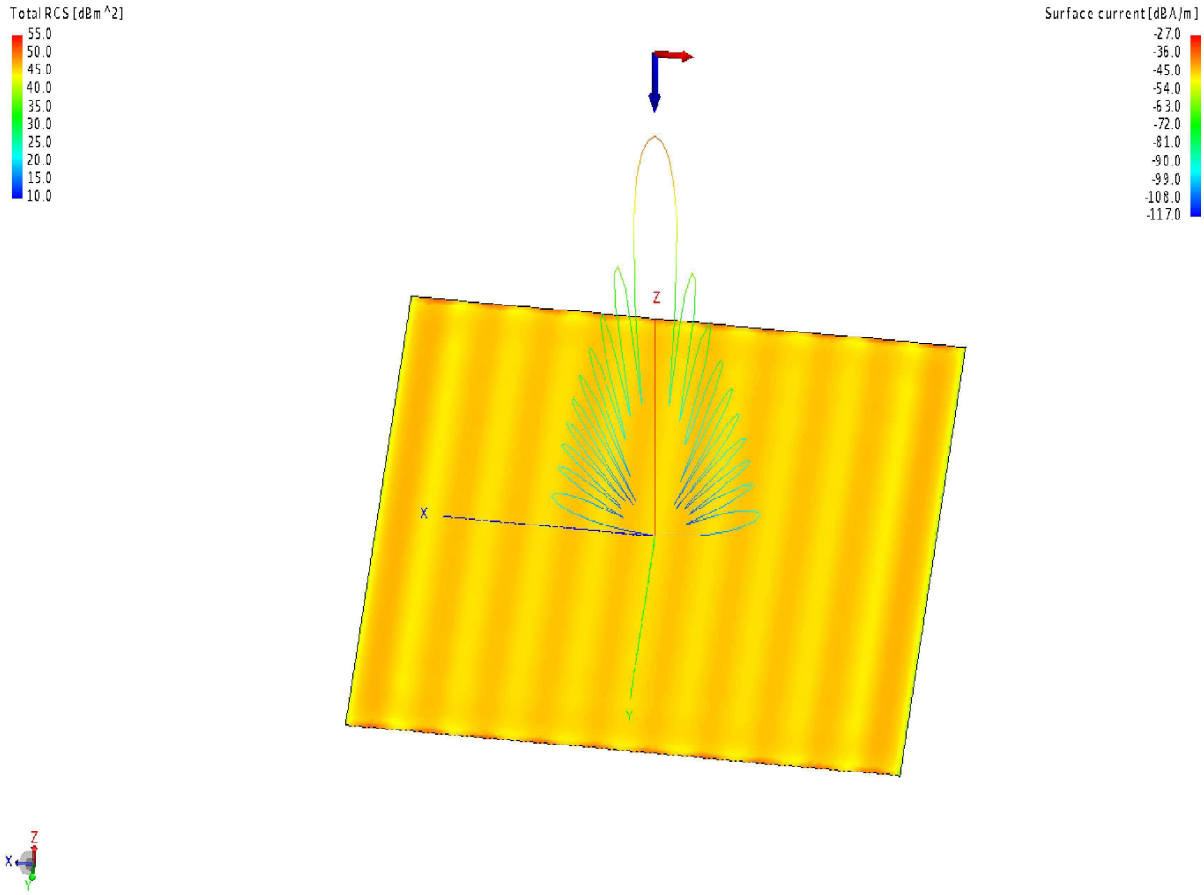

Figure 3.10: Current distribution and the RCS from square plate of dimension $10\lambda_0 \times 10\lambda_0$.

$M_{xx}c_x$ is written as

$$M_{xx}c_x(\mathbf{R}_i) = \sum_{j=0}^{N-1} \Big(\int\int_{Dj} G'(R_i)(z'_x u_{xi} + z_{yi} u_{yi} - u_{zi} \cdot dx'dy') \Big) c_{xj}$$
$$= \sum_{j=0}^{N-1} M_{xxij} c_{xj}, \tag{3.32}$$

In the same way, we can explain the other elements of M, which are M_{xy}, M_{yx}, M_{yy}. If the rough surface is described as a superposition of small planer surfaces, the elements at the Diagonal are small compared to the 1/2 term of the MFIE equation, because they depend on the

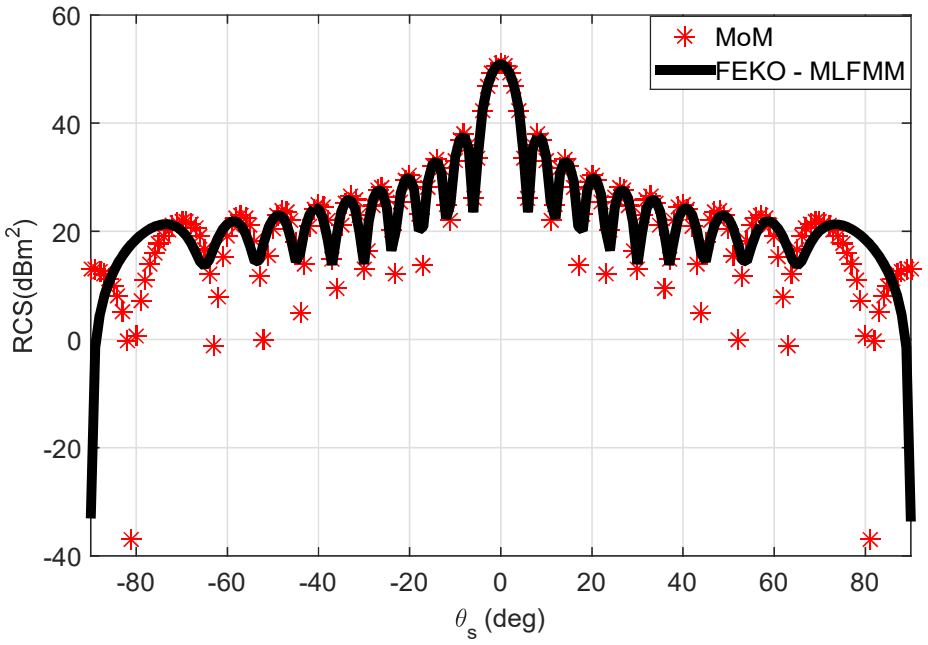

Figure 3.11: Comparison of the RCS from MoM and the results from FEKO for TE polarization, the square plate has dimensions $10\lambda_0 \times 10\lambda_0$, $\Delta x = \Delta y = \lambda_0/8$ $\theta_i = 0^o$, $\phi_i = 0^o$.

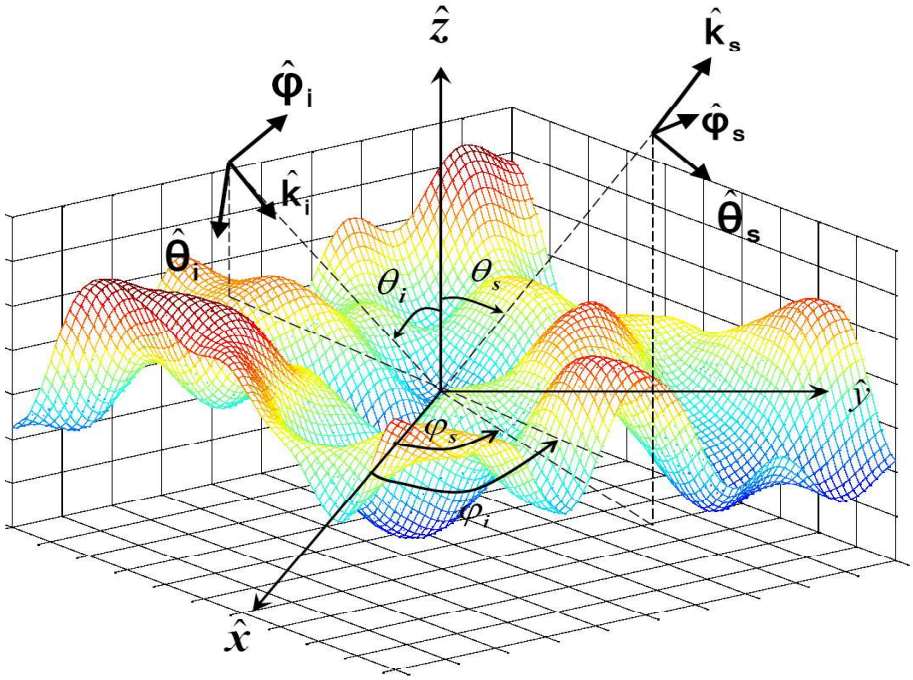

Figure 3.12: The geometry of the problem: the excitation of rough surface by plane wave.

curvature of the surface, the other element of the matrix can be computed

from

$$\begin{bmatrix} M_{xx} & M_{xy} \\ M_{yx} & M_{yy} \end{bmatrix} = \sum_{j=0}^{N-1} \frac{G'(R_{ij})}{R_{ij}} \begin{bmatrix} z_{xj}x_{ij} + z_{yi}y_{ij} - z_{ij} & (z_{yj} - z_{yi})x_{ij} \\ (z_{xj} - z_{xi})y_{ij} & z_{xi}x_{ij} + z_{yj}y_{ij} - z_{ij}\Delta x\Delta y. \end{bmatrix} \tag{3.33}$$

Finally, the linear system obtained from the MFIE for the problem of the electromagnetic scattering from a perfectly conductive rough surface is

$$\begin{bmatrix} M_{xx} & M_{xy} \\ M_{yx} & M_{yy} \end{bmatrix} \begin{bmatrix} \bar{\mathbf{J}}_x \\ \bar{\mathbf{J}}_y \end{bmatrix} = \begin{bmatrix} \bar{\mathbf{J}}_i^x \\ \bar{\mathbf{J}}_i^y \end{bmatrix} \tag{3.34}$$

Then the surface current can be calculated by inverting the impedance matrix in the form

$$\begin{bmatrix} \bar{\mathbf{J}}_x \\ \bar{\mathbf{J}}_y \end{bmatrix} = \begin{bmatrix} M_{xx} & M_{xy} \\ M_{yx} & M_{yy} \end{bmatrix}^{-1} \begin{bmatrix} \bar{\mathbf{J}}_i^x \\ \bar{\mathbf{J}}_i^y \end{bmatrix} \tag{3.35}$$

We tested the model of the case on a rough surface of the dimensions $8\lambda_0 \times 8\lambda_0$, then the RCS is then compared with the results we have for the same rough surface on FEKO.

The results of the proposed MoM and the results taken from FEKO software show good agreements at most scattered angles while the RCS at the edges shows some differences, these differences occurs because FEKO uses different IE's to solve the scattering equations, moreover, FEKO uses triangular bases functions in discritization, while this thesis used the rectangular basis functions, therefore, some differences are seen in the results.

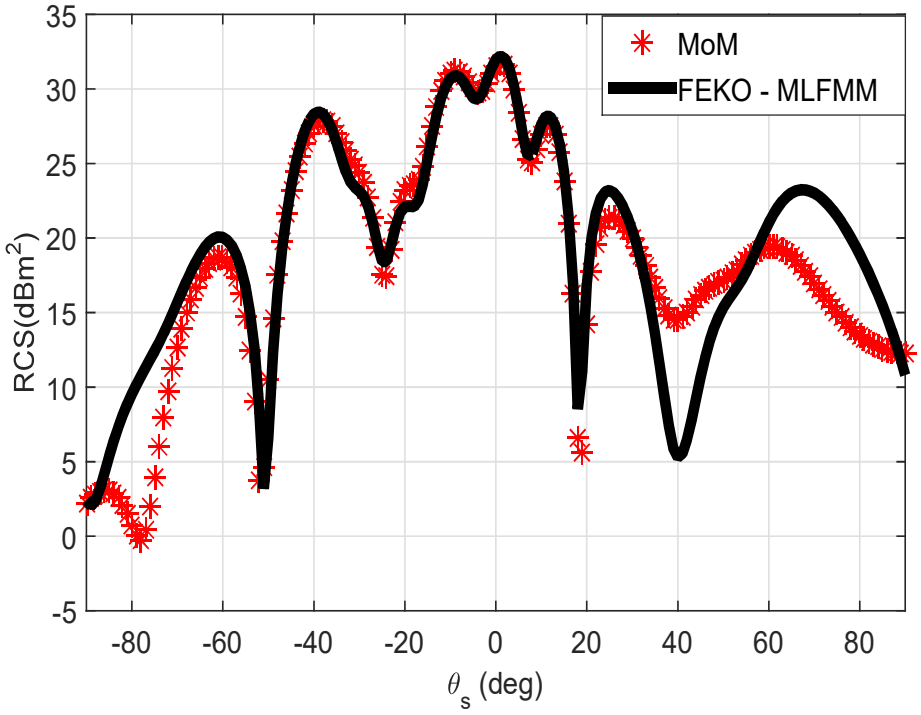

Figure 3.13: Comparison of the RCS from MoM and the results from FEKO for horizontal polarization, the rough surface has dimensions $8\lambda_0 \times 8\lambda_0$, $\Delta x = \Delta y = \lambda_0/8$ $\theta_i = 0^o$, $\phi_i = 0^o$.

3.3 Conclusion

In this chapter, we discussed the MoM and applied it for one scatterer in the case of electrostatic problems (charged thin wire and charged plate), and the case of scattering problems (square plat and rough surface). We discussed the result of the simulation of RCS for some scattering scenarios.

In the following chapter, we will apply MoM for two scatterers, in order to obtain a fast algorithm that takes into account the interaction between the two scatterers (object above rough surface).

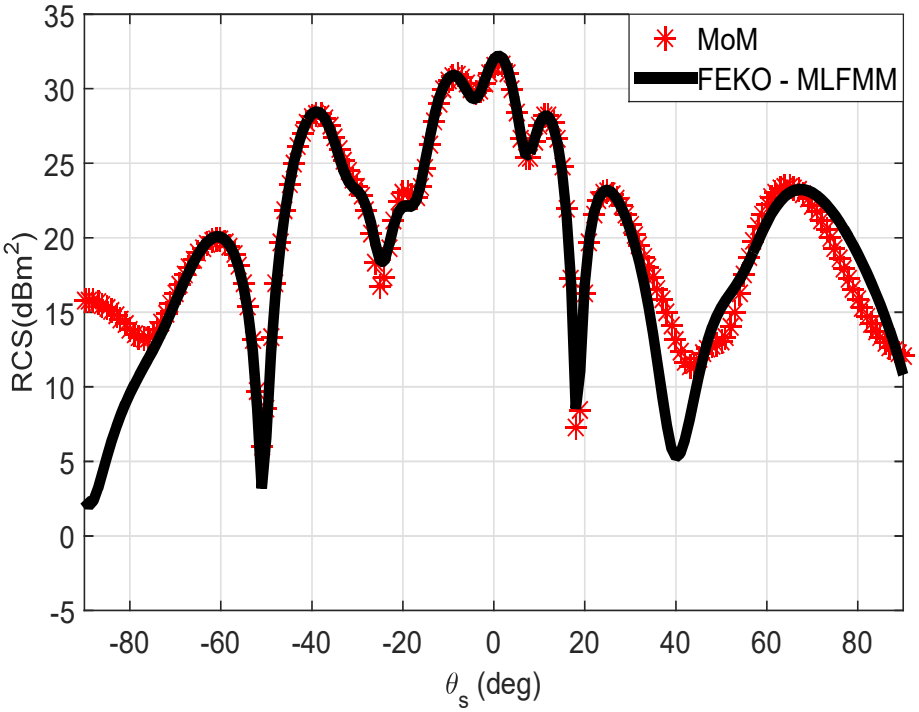

Figure 3.14: Comparison of the RCS from MoM and the results from FEKO for a vertical polarization, the rough surface has dimensions $8\lambda_0 \times 8\lambda_0$, $\Delta x = \Delta y = \lambda_0/8$ $\theta_i = 0^o$, $\phi_i = 0^o$.

Chapter 4

Electromagnetic Scattering from Two Scatterers

In this chapter, we discuss how to model the scattering between two 3D scatterers, especially the case of an object located above a rough surface. In this case, the interaction between the two scatterers should be considered. So that, we focus on the integral equations of this case, and apply MoM to solve them as done in the previous chapter. Later, some approximating methods are used to accelerate the computations. MoM solution is considered as the reference exact solution for this problem.

Later in this chapter, we are going to introduce the integral equations for two scatterers, and discuss the discretization using MoM, then an explanation in details for E-PILE method is discussed and how to use it in MoM. Finally, we accelerate the computations using Physical Optics method with Adaptive Cross Approximation. The scenarios of two parallel plates in free space and square plate above the rough surface are tested to validate the model.

4.1 Integral Equations for two scatterers

In the previous chapter, we studied the scattered field from a single scatterer for two cases, square plate and rough surface, each one alone. We solved the IE's for these cases and applied MoM to solve them. In this chapter, we can not deal with the scenario of two scatterers in the same way, because the coupling between the two surfaces occurs, the resulting scattered field is not the sum of the scattered field from each surface as if it is isolated from the other object, so the coupling is taken in account in the integral equations and the solution of this problem.

To begin, consider the scenario given in Figure 4.1, the source is located in medium Ω_0 with permittivity ϵ_0, in volume V_0. This medium contains two scatterers, scatterer 1 with permittivity ϵ_1, and volume V_1, and scatterer 2 with with permittivity ϵ_2, and volume V_2. S_1 represents the surface surrounding V_1, n_1 is the normal to S_1 and is pointing towards the outside of V_1 (towards the incident medium), and S_2 is the surface surrounding V_2, and $\hat{\mathbf{n}}_2$ is the normal to S_2 is pointing towards the outside of V_2. S_∞ is the surface surrounding the incident medium, $\hat{\mathbf{n}}_\infty$ is pointing outside V_0.

Applying the boundary conditions, the integral equation of the first scatterer $\forall \quad \mathbf{R}_1, \mathbf{R}' \in S_1$ and $\forall \quad \mathbf{R}_2 \in S_2$

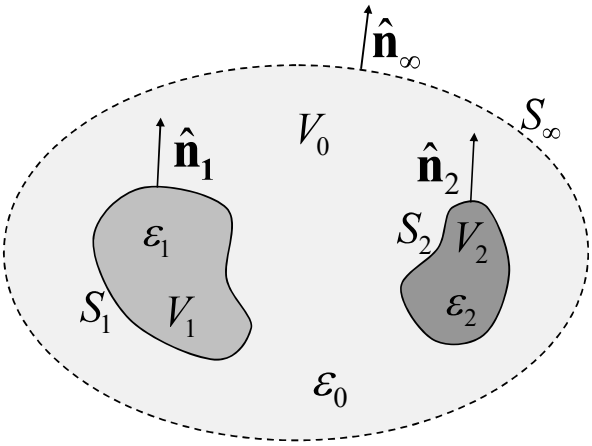

Figure 4.1: Two scatterers located in volume V_0

$$\frac{1}{2}\mathbf{J}_1(\mathbf{R}') = \hat{\mathbf{n}}_1(\mathbf{R}') \times \mathbf{H}_i(\mathbf{R}') + \underbrace{\hat{\mathbf{n}}_1(\mathbf{R}') \times \oint_{S_1} \mathbf{J}_1(\mathbf{R}_1) \times \boldsymbol{\nabla}_{\mathbf{R}_1} G(\mathbf{R}_1, \mathbf{R}') \cdot ds}_{\text{Local Interaction}}$$
$$+ \underbrace{\hat{\mathbf{n}}_1(\mathbf{R}') \times \oint_{S_2} \mathbf{J}_2(\mathbf{R}_2) \times \boldsymbol{\nabla}_{\mathbf{R}_2} G(\mathbf{R}_2, \mathbf{R}') \cdot ds}_{\text{Coupling}} \quad (4.1)$$

In the same way, the integral equation of the second scatterer $\forall \mathbf{R}_2, \mathbf{R}' \in S_2$ and $\forall \mathbf{R}_1 \in S_1$

$$\frac{1}{2}\mathbf{J}_2(\mathbf{R}') = \hat{\mathbf{n}}_2(\mathbf{R}') \times \mathbf{H}_i(\mathbf{R}') + \underbrace{\hat{\mathbf{n}}_2(\mathbf{R}') \times \oint_{S_2} \mathbf{J}_2(\mathbf{R}_2) \times \boldsymbol{\nabla}_{\mathbf{R}_2} G(\mathbf{R}_2, \mathbf{R}') \cdot ds}_{\text{Local Interaction}}$$
$$+ \underbrace{\hat{\mathbf{n}}_2(\mathbf{R}') \times \oint_{S_1} \mathbf{J}_1(\mathbf{R}_1) \times \boldsymbol{\nabla}_{\mathbf{R}_1} G(\mathbf{R}_1, \mathbf{R}') \cdot ds}_{\text{Coupling}} \quad (4.2)$$

Where $\mathbf{R}_1, \mathbf{R}_2$ are any point located at the scatterer 1 and scatterer 2 respectively. The symbol $\oint$ refers to the Cauchy principle, which means

that the integration is not calculated in the case where the source point is the same as the test point ($\mathbf{R}_1, \mathbf{R}_2 \neq \mathbf{R}'$).

We can explain equations 4.1, 4.2 as the total current in the surface lets take S_1 as an example, the total current is the current from the incident wave and the surface current that occurs in the surface and the current that produced as a result of the interaction occurs because of the second scatterer.

In this integral equations, we have two unknowns to be found, the surface current at the first scatterer ($\mathbf{J}_1$) and the surface current at the second scatterer ($\mathbf{J}_2$). To solve this problem, the MoM will be applied.

4.2 Discretization by Method of Moment

In order to solve the integral equations for two scatterers using MoM, we first discretize the two surfaces, each surface is divided into small segments, then the surface current is calculated at each segment. We will use the pulse function as the basis functions and delta functions as the test functions. The result of applying MoM is a linear system of the form $\bar{\mathbf{Z}}\mathbf{X} = \mathbf{b}$, this linear system describes the total scene we have. In details, the unknown vector $\mathbf{X}$ contains all the unknown current surface

for scatterer 1 and scatterer 2 in the form

$$\mathbf{X} = \begin{bmatrix} \mathbf{X}_1 \\ \\ \mathbf{X}_2 \end{bmatrix} \tag{4.3}$$

Where $\mathbf{X}_1$ is the surface current on the first scatterer, and $\mathbf{X}_2$ contains the surface currents for the second scatterer. $\mathbf{X}_1, \mathbf{X}_2$ are expanded in the form

$$\mathbf{X}_1 = \begin{bmatrix} \mathbf{J}_1(\mathbf{R}_1^1) \\ \mathbf{J}_1(\mathbf{R}_1^2) \\ \vdots \\ \mathbf{J}_1(\mathbf{R}_1^{N_1}) \end{bmatrix} \tag{4.4}$$

$$\mathbf{X}_2 = \begin{bmatrix} \mathbf{J}_2(\mathbf{R}_2^1) \\ \mathbf{J}_2(\mathbf{R}_2^2) \\ \cdots \\ \mathbf{J}_2(\mathbf{R}_2^{N_2}) \end{bmatrix} \tag{4.5}$$

Here, N_1, N_2 are the number of unknowns in the first and second scatterer respectively. As can be noticed, $\mathbf{X}$ vector has a dimension of $(N_1+N_2)\times 1$. For our 3D problem, the current on each segment should represent the $\hat{\mathbf{x}}, \hat{\mathbf{y}}, \hat{\mathbf{z}}$ components of the current, so $\mathbf{J}_1(\mathbf{R}_1) = J_{x_1}\hat{\mathbf{x}} + J_{y_1}\hat{\mathbf{y}} + J_{z_1}\hat{\mathbf{z}}$ and $\mathbf{J}_2(\mathbf{R}_2) = J_{x_2}\hat{\mathbf{x}} + J_{y_2}\hat{\mathbf{y}} + J_{z_2}\hat{\mathbf{z}}$.

The column vector $\mathbf{b}$ which represents the incident field is equal to ($\mathbf{b} =$

$\hat{\mathbf{n}} \times \mathbf{H}_i$) has a dimension of $((N_1 + N_2) \times 1)$ and is described as

$$\mathbf{b} = \begin{bmatrix} \mathbf{b}_1 \\ \\ \mathbf{b}_2 \end{bmatrix} \tag{4.6}$$

where $\mathbf{b}_1, \mathbf{b}_2$ are the incident wave on the scatterer 1 and scatterer 2 respectively.

The impedance matrix $\bar{\mathbf{Z}}$ represents the impedance matrix for the whole scene, its dimension is $(N_1 + N_2) \times (N_1 + N_2)$, $\bar{\mathbf{Z}}$ can be expressed as a matrix of the sub matrices in the form

$$\bar{\mathbf{Z}} = \begin{bmatrix} \bar{\mathbf{Z}}_1 & \bar{\mathbf{Z}}_{12} \\ \bar{\mathbf{Z}}_{21} & \bar{\mathbf{Z}}_2 \end{bmatrix} \tag{4.7}$$

Here $\bar{\mathbf{Z}}_1$ is the impedance matrix for the first scatterer occurs from the local interaction on its surface alone as if it is in free space, in other words, the impedance matrix without any effects of the existence of the other scatterer. Moreover, $\bar{\mathbf{Z}}_{21}$ is the impedance matrix that describes the coupling between the two scatterers. In the same way, $\bar{\mathbf{Z}}_2$ is the impedance matrix of the second scatterer without any effects of the first scatterer and $\bar{\mathbf{Z}}_{21}$ describes the effect of the coupling happens because of the first scatterer.

To summarize, the linear system of the form $\bar{\mathbf{Z}}\mathbf{X} = \mathbf{b}$ is represents on

the form of

$$\begin{bmatrix} \bar{\mathbf{Z}}_1 & \bar{\mathbf{Z}}_{12} \\ \bar{\mathbf{Z}}_{21} & \bar{\mathbf{Z}}_2 \end{bmatrix} \begin{bmatrix} \mathbf{X}_1 \\ \mathbf{X}_2 \end{bmatrix} = \begin{bmatrix} \mathbf{b}_1 \\ \mathbf{b}_2 \end{bmatrix} \tag{4.8}$$

The direct way to solve this system is to find $\bar{\mathbf{Z}}^{-1}$ and multiply it with $\mathbf{b}$, then $\mathbf{X} = \bar{\mathbf{Z}}^{-1}\mathbf{b}$. This solution is acceptable when the size of $\bar{\mathbf{Z}}$ is small, and this is limited to small electrical scatterers. A direct solution divides the impedance matrix into two parts called Lower and Upper (MoM-LU), then do the calculations , the MoM-LU will be taken as the reference solution for our results, since it is an exact solution for the system $\mathbf{X} = \bar{\mathbf{Z}}\mathbf{b}$. The RCS from the proposed methods will be tested and compared with RCS occurs from the MoM-LU.

As the size of the impedance matrix increase, the memory needed and the computational time for the inverse of $\bar{\mathbf{Z}}$ rise rapidly making it not an efficient way. Recently, an attractive method called E-PILE were used to enhance these calculations, E-PILE method is discussed in the following section.

4.3 Extended Propagation Inside Layer Expansion (E-PILE)

As discussed in the previous chapter, the direct method to solve the linear system of the form $\bar{\mathbf{Z}}\mathbf{X} = \mathbf{b}$ is to find the inverse of $\bar{\mathbf{Z}}$ matrix then multiply it by the vector $\mathbf{b}$ in the form of $\mathbf{X} = \bar{\mathbf{Z}}^{-1}\mathbf{b}$, This way requires huge memory. A fast method called Propagation Inside Layer

Expansion (PILE) was developed in [13], this method suggests a fast solution depends on dividing the impedance matrix $\bar{\mathbf{Z}}$ into submatrices. So, instead of invert an $(N_1 + N_2) \times (N_1 + N_2)$ matrix, it calculates $\bar{\mathbf{Z}}^{-1}$ by other formula, as will be discussed later in this section. Then, they applied the new proposed method to two one-dimensional interfaces, only one of them is illuminated by a plane wave. Later in [14], PILE was extended for the general case, where the two scatterers are illuminated, also the proposed method is applied to an object above a one-dimensional rough surface.

E-PILE divides the impedance matrix into sub-matrices, then calculates the inverse of it by the:

$$\bar{\mathbf{Z}}^{-1} = \begin{bmatrix} \bar{\mathbf{T}} & \bar{\mathbf{U}} \\ \bar{\mathbf{V}} & \bar{\mathbf{W}} \end{bmatrix} \tag{4.9}$$

Where $\bar{\mathbf{T}}, \bar{\mathbf{U}}, \bar{\mathbf{V}}$ and $\bar{\mathbf{W}}$ are sub matrices obtained as following

$$\begin{cases} \bar{\mathbf{T}} = (\bar{\mathbf{Z}}_1 - \bar{\mathbf{Z}}_{21}\bar{\mathbf{Z}}_2^{-1}\bar{\mathbf{Z}}_{12})^{-1}, \\ \bar{\mathbf{U}} = -(\bar{\mathbf{Z}}_1 - \bar{\mathbf{Z}}_{21}\bar{\mathbf{Z}}_2^{-1}\bar{\mathbf{Z}}_{12})^{-1}, \\ \bar{\mathbf{V}} = -\bar{\mathbf{Z}}_2^{-1}\bar{\mathbf{Z}}_{12}(\bar{\mathbf{Z}}_1 - \bar{\mathbf{Z}}_{21}\bar{\mathbf{Z}}_2^{-1}\bar{\mathbf{Z}}_{12})^{-1}, \\ \bar{\mathbf{W}} = \bar{\mathbf{Z}}_2^{-1} + \bar{\mathbf{Z}}_2^{-1}\bar{\mathbf{Z}}_{12}(\bar{\mathbf{Z}}_1 - \bar{\mathbf{Z}}_{21}\bar{\mathbf{Z}}_2^{-1}\bar{\mathbf{Z}}_{12})^{-1}\bar{\mathbf{Z}}_{21}Z_2^{-1}, \end{cases} \tag{4.10}$$

As shown from the previous expression, the inverse of submatrices should be calculated. However, it is clear that the computation time and memory used to compute the inverse of the matrix of dimension $N_1 + N_2$ are

huge compared of the time requires finding the inverse of the matrix of dimension N_1 or N_2. Substituting the values in the system $\mathbf{X} = \bar{\mathbf{Z}}^{-1}\mathbf{b}$ leads to

$$\begin{bmatrix} \mathbf{X}_1 \\ \mathbf{X}_2 \end{bmatrix} = \bar{\mathbf{Z}}^{-1} \begin{bmatrix} \mathbf{b}_1 \\ \mathbf{b}_2 \end{bmatrix} = \begin{bmatrix} \bar{\mathbf{T}}\mathbf{b}_1 + \bar{\mathbf{U}}\mathbf{b}_2 \\ \bar{\mathbf{V}}\mathbf{b}_1 + \bar{\mathbf{W}}\mathbf{b}_2 \end{bmatrix}, \tag{4.11}$$

From equation 4.11, $\mathbf{X}_1 = \bar{\mathbf{T}}\mathbf{b}_1 + \bar{\mathbf{U}}\mathbf{b}_2$, substituting $\bar{\mathbf{T}}$ and $\bar{\mathbf{U}}$, we have

$$\mathbf{X}_1 = (\bar{\mathbf{Z}}_1 - \bar{\mathbf{Z}}_{21}\bar{\mathbf{Z}}_2^{-1}\bar{\mathbf{Z}}_{12})^{-1}\mathbf{b}_1 - (\bar{\mathbf{Z}}_1 - \bar{\mathbf{Z}}_{21}\bar{\mathbf{Z}}_2^{-1}\bar{\mathbf{Z}}_{12})^{-1}\bar{\mathbf{Z}}_{21}\bar{\mathbf{Z}}_2^{-1}\mathbf{b}_2, \tag{4.12}$$

Equation 4.12 can be written in the form of

$$\mathbf{X}_1 = (\bar{\mathbf{Z}}_1 - \bar{\mathbf{Z}}_{21}\bar{\mathbf{Z}}_2^{-1}\bar{\mathbf{Z}}_{12})^{-1}[\mathbf{b}_1 - \bar{\mathbf{Z}}_{21}\bar{\mathbf{Z}}_2^{-1}\mathbf{b}_2], \tag{4.13}$$

Now, we introduce the characteristic matrix $\bar{\mathbf{M}}_{c,1}$ as

$$\bar{\mathbf{M}}_{c,1} = \bar{\mathbf{Z}}_1^{-1}\bar{\mathbf{Z}}_{21}\bar{\mathbf{Z}}_2^{-1}\bar{\mathbf{Z}}_{12}, \tag{4.14}$$

then

$$\mathbf{X}_1 = (\bar{\mathbf{I}} - \bar{\mathbf{M}}_{c,1})^{-1}\bar{\mathbf{Z}}_1^{-1}(\mathbf{b}_1 - \bar{\mathbf{Z}}_{21}\bar{\mathbf{Z}}_2^{-1}\mathbf{b}_2), \tag{4.15}$$

where $\bar{\mathbf{I}}$ is the identity matrix.

The first part of equation 4.15 can be expanded using Taylor series to be

$$(\bar{\mathbf{I}} - \bar{\mathbf{M}}_{c,1})^{-1} = [\sum_{p=0}^{p=\infty} \bar{\mathbf{M}}_{c,1}^{p}] \tag{4.16}$$

In this case a condition of $\left\|\bar{\mathbf{M}}_{c,1} < 1\right\|$ should be satisfied, where $\|\bullet\|$ is the normal of the matrix $\bar{\mathbf{M}}_{c,1}$ and equals to the maximum of the module of

its eigenvalues. To calculate numerically the summation in the previous equation, we truncation the summation at $p = P_{E-PILE}$, then we obtain

$$\mathbf{X}_1 = \Big[\sum_{p=0}^{p=P_{E-PILE}} \bar{\mathbf{M}}_{c,1}^{p} \Big] \bar{\mathbf{Z}}_1^{-1} (\mathbf{b}_1 - \bar{\mathbf{Z}}_{21} \bar{\mathbf{Z}}_2^{-1} \mathbf{b}_2) = \sum_{p=0}^{p=P_{E-PILE}} \mathbf{Y}_1^{(p)}, \quad (4.17)$$

where

$$\begin{cases} \mathbf{Y}_1^0 = \bar{\mathbf{Z}}_1^{-1} (\mathbf{b}_1 - \bar{\mathbf{Z}}_{21} \bar{\mathbf{Z}}_2^{-1} \mathbf{b}_2), & p = 0 \\ \mathbf{Y}_1^{(p)} = \bar{\mathbf{M}}_{c,1} \mathbf{Y}_1^{(p-1)}, & p > 0 \end{cases} \quad (4.18)$$

In the same way, we can find the surface current at the second scatterer $\mathbf{X}_2$ by replacing the index $1, 2, 12, 21$ by $2, 1, 21, 12$ respectively in equations 4.17, 4.18, 4.16, 4.15, the characteristic matrix for the second scatterer surface is

$$\bar{\mathbf{M}}_{c,2} = \bar{\mathbf{Z}}_2^{-1} \bar{\mathbf{Z}}_{12} \bar{\mathbf{Z}}_1^{-1} \bar{\mathbf{Z}}_{21}, \quad (4.19)$$

Recall that the $\bar{\mathbf{Z}}_1$ is the impedance matrix of the first scatterer as if it is in the free space, $\bar{\mathbf{Z}}_2$ is the impedance matrix of the second scatterer when it is isolated (in free space), and $\bar{\mathbf{Z}}_{21}, \bar{\mathbf{Z}}_{12}$ are the coupling matrices occurs because of the interaction between the two scatterers. To have a physical meaning of the previous equations, Figure 4.2 will help to illustrate the discussion.

In the zeroes order term, $\bar{\mathbf{Z}}_1^{-1}$ accounts for the total interactions on the first scatterer, $\mathbf{Y}_1^{(0)}$ correspondent to the contribution on the object, when it is illuminated by the direct incident field ($\mathbf{b}_1$) and the direct scattered field by the rough surface ($-\bar{\mathbf{Z}}_{21} \bar{\mathbf{Z}}_2^{-1} \mathbf{b}_2$). In the first order term,

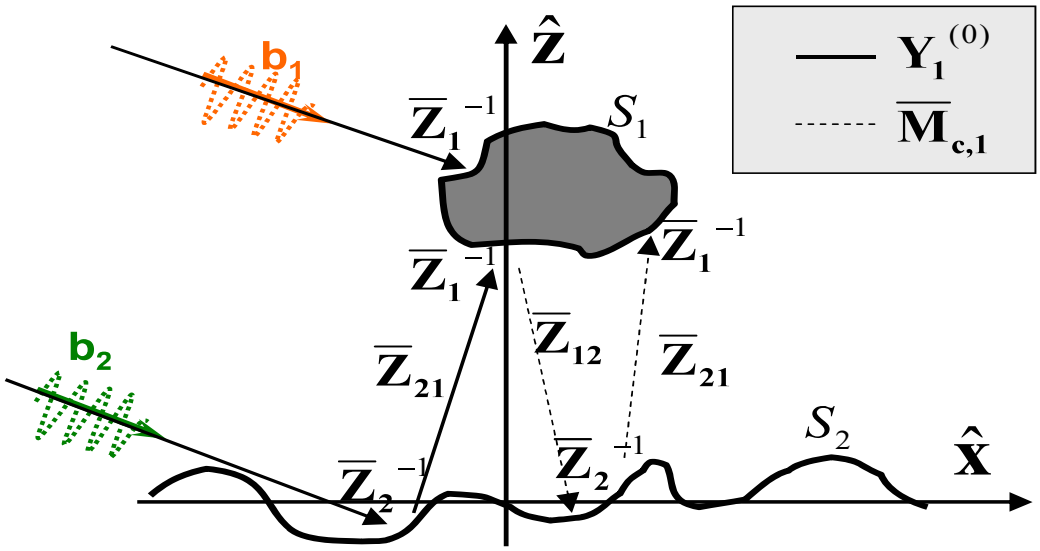

Figure 4.2: Physical interpretation of E-PILE method.

$\mathbf{X}_1^{(1)} = \bar{\mathbf{M}}_{c,1}\mathbf{X}_1^0$, $\bar{\mathbf{Z}}_{12}$ propagates the resulting object field information, $\mathbf{X}_1^0$, toward the rough surface, $\bar{\mathbf{Z}}_2^{-1}$ accounts for the local interactions on the second scatterer, and $\bar{\mathbf{Z}}_{21}$ re-propagates the resulting contribution toward the object, finally $\bar{\mathbf{Z}}_1^{-1}$ updates the field values on the object. So the characteristic matrix $\bar{\mathbf{M}}_{c,1}$ realize a back and forth between the object and the rough surface. The number of the back and forth interaction between the object and the rough surface is determined by the P_{E-PILE}. In the same way, $\bar{\mathbf{M}}_{c,2}$ corresponds a back and forth interactions between the rough surface and the object.

To study the effect of the order of E-PILE, the RCS of order 0, 3 and 8 are computed then compared with the RCS computed from MoM-LU for two scenarios, the first is two parallel square plates and the second scenario is for a square plate located above rough surface for two incident angels $\theta_i = 0, 45$.

For scenario 1, consider two parallel plates, the first plate is of dimension

$2\lambda_0 \times 2\lambda_0$, and the second plate is of dimension of $6\lambda_0 \times 6\lambda_0$. The two plates are separated by a distance of $5\lambda_0$ as shown in Figure 4.3. Each segment of the two scatterers is of dimension $\Delta x = \Delta y = \lambda_0/8$, the incident wave is at angle of $\theta_i = 0^o$. The RCS for E-PILE of order 0, 3 and 8 compared with MoM-LU is shown in Figure 4.4.

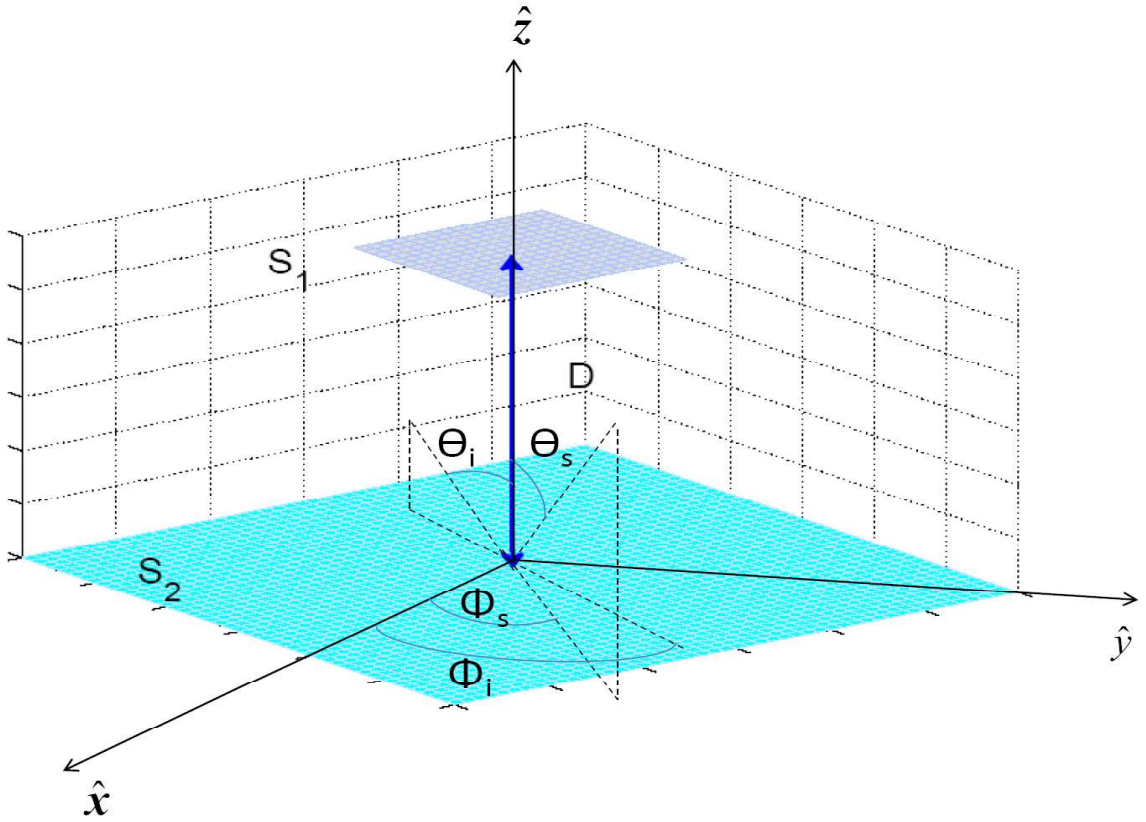

Figure 4.3: The geometry of two parallel plates.

Figure 4.5 shows the RCS for scenario 1 at incident angle $\theta_i = 45^o$.

As shown in Figures 4.4, 4.5, increasing the order of E-PILE leads to fast converges to the results of MoM-LU (order 8 is closer to MoM-LU than order 0), if we suppose the threshold of the error to be 0.002, then as [39], order 6 gives that threshold. From this point we would use order 6 as the chosen order to compare with other methods.

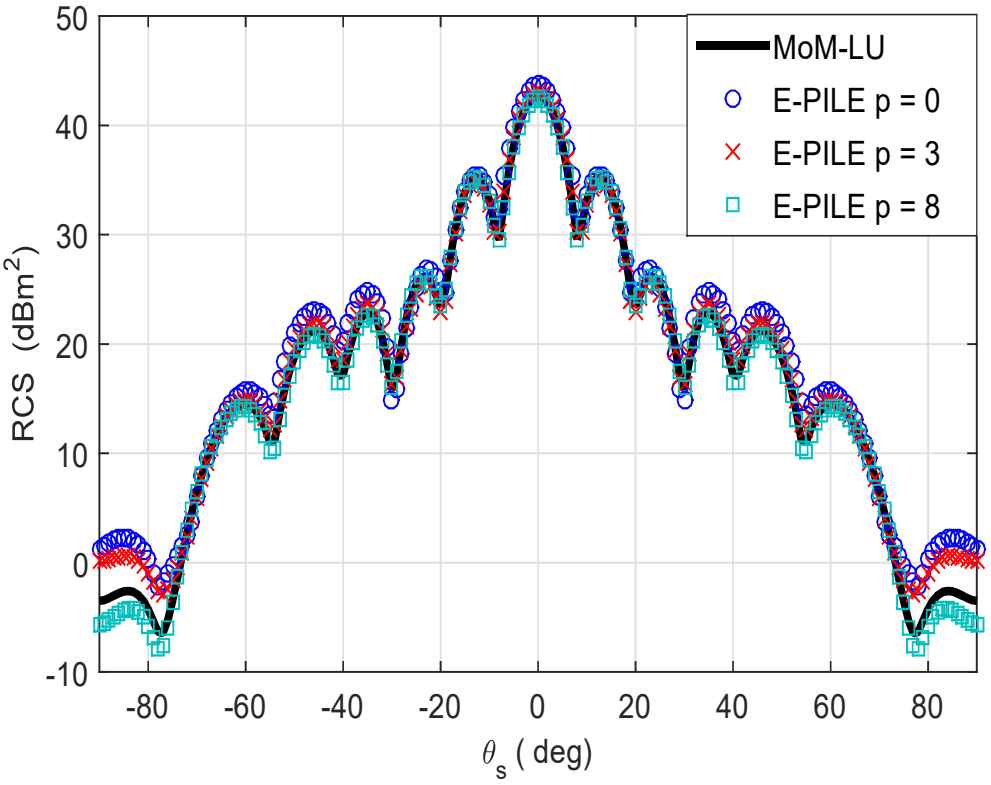

Figure 4.4: The RCS for two parallel plates computed by MoM-LU and E-PILE of order 0, 3 and 8, the plates are at dimensions of $2\lambda_0 \times 2\lambda_0$ and $6\lambda_0 \times 6\lambda_0$, separated by distance of $5\lambda_0$, and illuminated by plane wave at an incident angle of $\theta_i = 0^o$.

For scenario 2, consider a square plate of dimension $2\lambda_0 \times 2\lambda_0$ is located above rough surface with dimension of $8\lambda_0 \times 8\lambda_0$, as shown in Figure 4.6. The two scatterers are separated by distance of $5\lambda_0$, each segment of the two scatterers is of dimension $\Delta x = \Delta y = \lambda_0/8$, the incident wave is at angle of $\theta_i = 0^o$. The RCS for E-PILE or order 0, 3 and 8 compared with MoM-LU is shown in Figure 4.7.

Figure 4.8 shows the RCS for the same previous scenario but at incident angle of 45. The results ensure the results we have in the case of the two parallel plates. It is clearly shown that the RCS for order 8 is almost the same as the RCS of MoM-LU for any incident angles. The higher the order of E-PILE, the better agreements and matching of the results

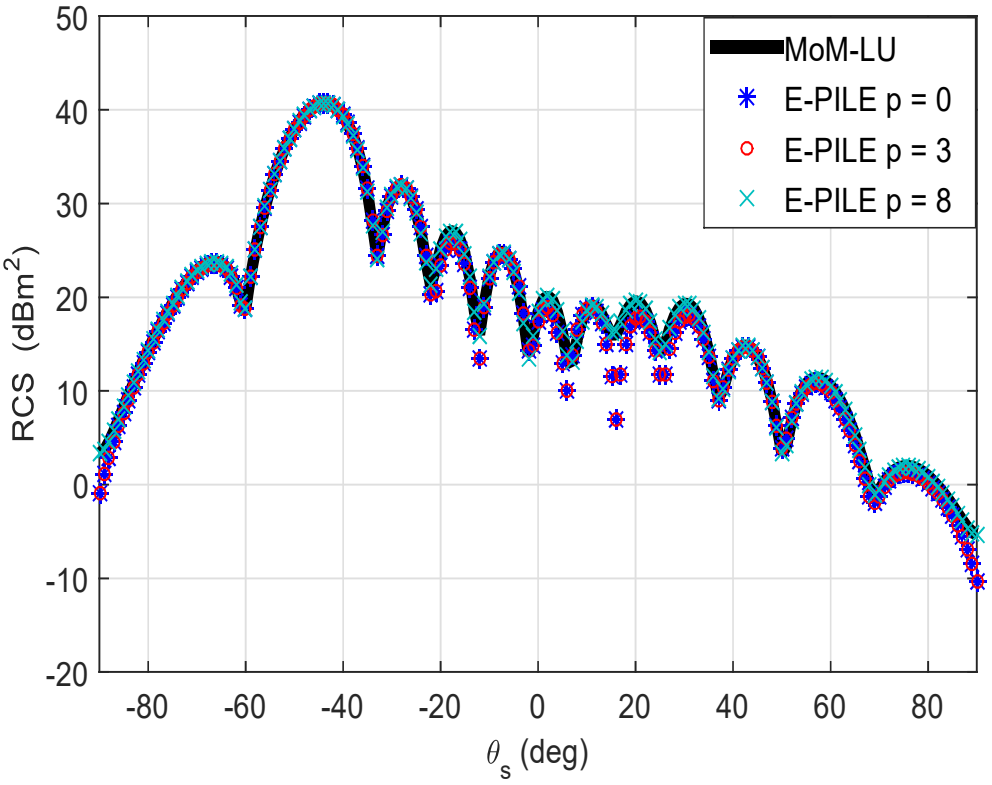

Figure 4.5: The RCS for two parallel plates computed by MoM-LU and E-PILE of order 0, 3 and 8, the plates are at dimensions of $2\lambda_0 \times 2\lambda_0$ and $6\lambda_0 \times 6\lambda_0$, separated by distance of $5\lambda_0$, and illuminated by plane wave at an incident angle of $\theta_i = 45^o$.

with the results of the reference method MoM-LU.

As the size of the scenario increases, time required to have the results becomes too long. E-PILE method proposed a very attractive method to solve the linear system $\bar{\mathbf{Z}}\mathbf{X} = \mathbf{b}$, but this method is still limited to the large electrically size scatterers, the need to accelerate the computations leads to use some approximated methods. One of the approximated methods called Physical Optics (PO), PO gives approximations that accelerates the computations with a very similar results. PO is discussed in the following section.

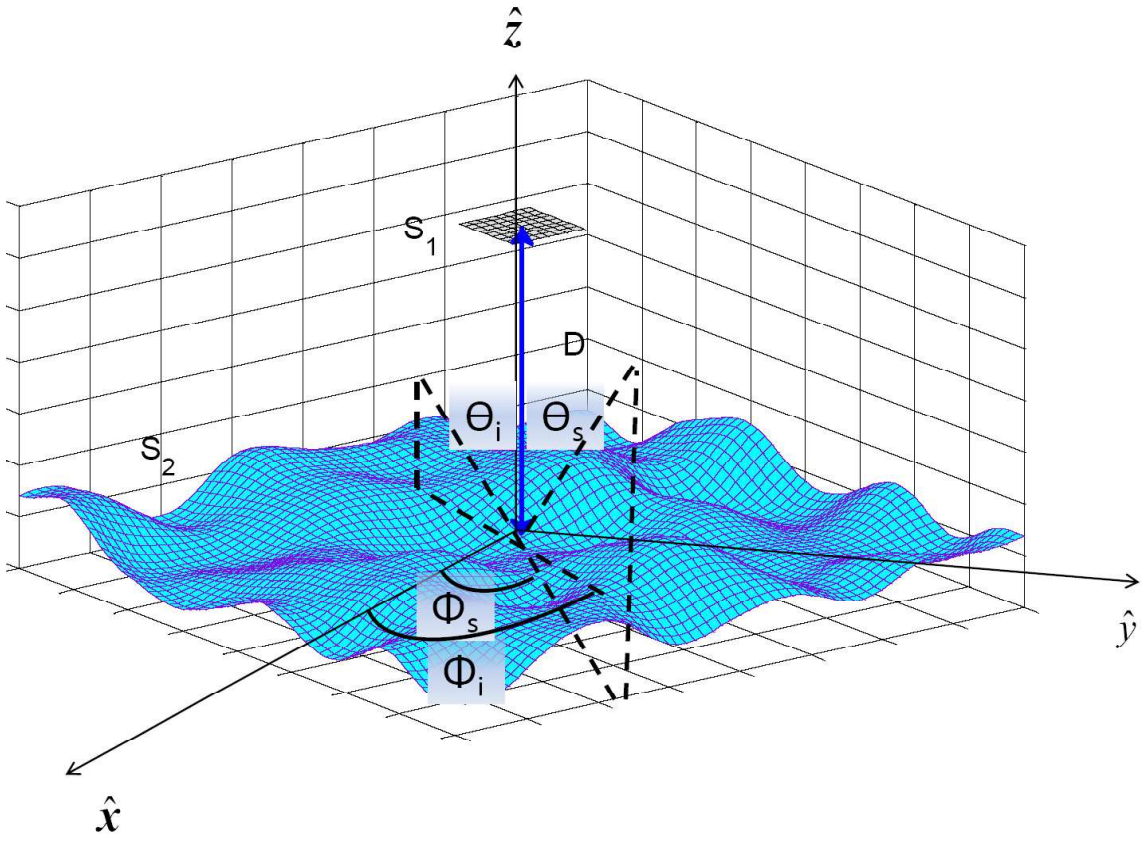

Figure 4.6: The geometry of square plate above rough surface.

4.4 Physical Optics

Physical Optics (PO) is an approximated method based on simplifying the integral equations. PO approximate the surface current on the object by the tangential field of the geometric optics. PO does not take into account the shadowing phenomenon and the discontinuity of the surface, this makes PO applications limited to surfaces with few roughness and close to be smooth. However, this simplification done by PO approximation prevents several complex calculations making the computations of the scattered field less complicated than computations in the case of exact methods like MoM, keeping an acceptable percentage of error in the results.

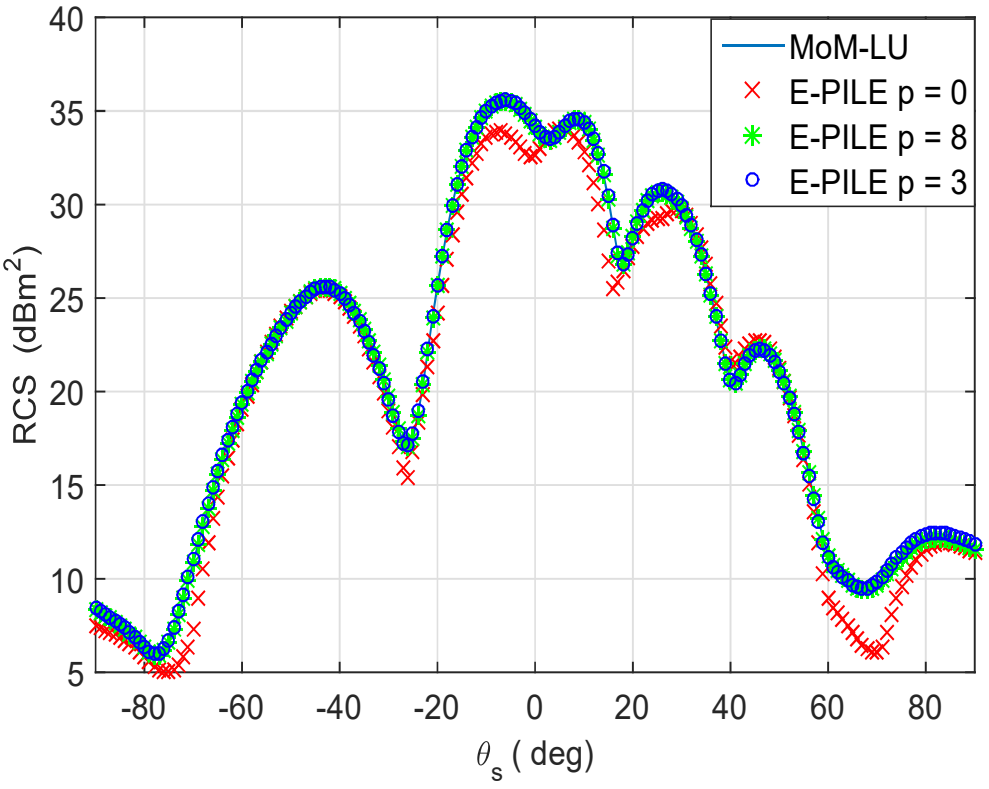

Figure 4.7: The RCS of plate above rough surface computed by MoM-LU and E-PILE of order 0, 3 and 8, the two scatterers are at dimensions of $2\lambda_0 \times 2\lambda_0$ and $8\lambda_0 \times 8\lambda_0$, separated by distance of $5\lambda_0$, and illuminated by plane wave at an incident angle of $\theta_i = 0^o$.

Consider the case of two different media, the first medium is PEC and the second medium with permittivity ϵ_1, permeability μ_1 and conductivity σ_1, the normal to the boundary surface ($\hat{\mathbf{n}}$) is pointing towards the second medium.

When the two media are illuminated by a plane wave, the incident electric field $\mathbf{E}_{i1}$ and the incident magnetic field $\mathbf{H}_{i1}$ will be vanish inside the PEC medium ($\mathbf{E}_{i1} = \mathbf{H}_{i1} = 0$), on the other side, the total field inside the second medium $\mathbf{E}_{tot}$ and $\mathbf{H}_{tot}$ are the summation of the incident fields and the reflected fields inside the second medium, ($\mathbf{E}_{tot} = \mathbf{E}_i + \mathbf{E}_r, \mathbf{H}_{tot} = \mathbf{H}_i + \mathbf{H}_r$), the electric and magnetic surface

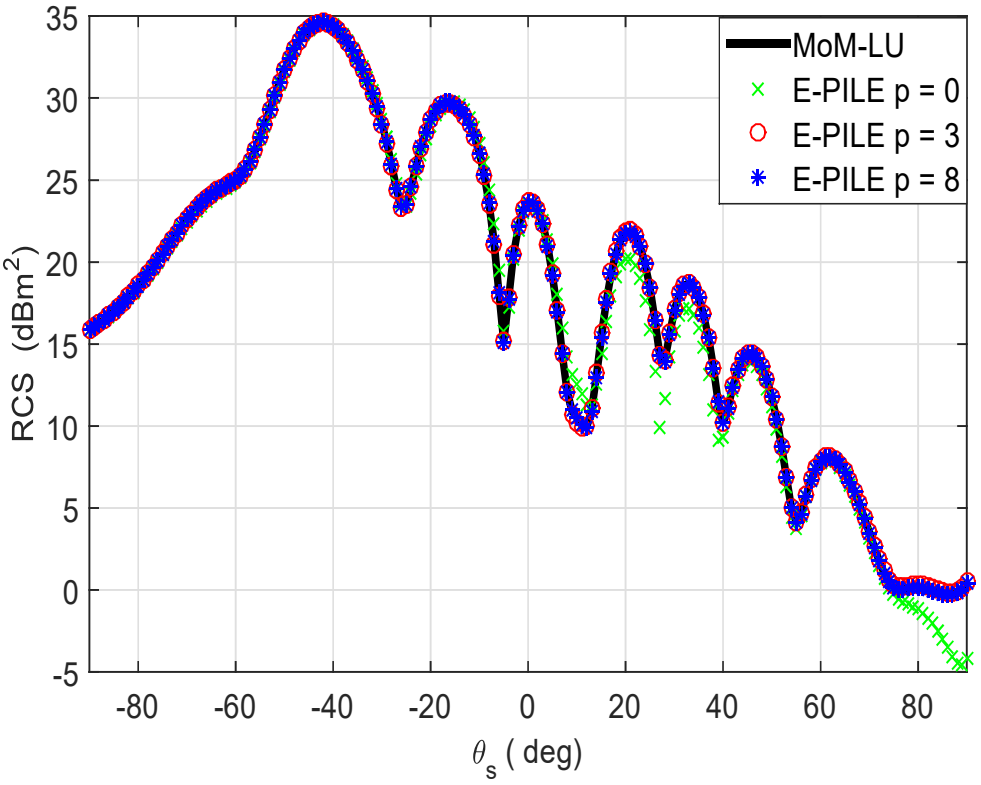

Figure 4.8: The RCS of plate above rough surface computed by MoM-LU and E-PILE of order 0, 3 and 8, the two scatterers are at dimensions of $2\lambda_0 \times 2\lambda_0$ and $8\lambda_0 \times 8\lambda_0$, separated by distance of $5\lambda_0$, and illuminated by plane wave at an incident angle of $\theta_i = 45^o$.

current densities $(\mathbf{J}, \mathbf{M})$ at the boundary can be obtained from the tangential components of the total fields

$$\mathbf{J} = \hat{\mathbf{n}} \times (\mathbf{H}_{tot1} - \mathbf{H}_{PEC-tot}) \mid_S = \hat{\mathbf{n}} \times \mathbf{H}_{tot1} \mid_S = \hat{\mathbf{n}} \times (\mathbf{H}_{i1} + \mathbf{H}_{r1}) \mid_S, \quad (4.20)$$

The physical optics approximation supposes that $\mathbf{H}_{i1}$ and $\mathbf{H}_{r1}$ at the boundary are at the same amplitude and same phase. So, the magnetic current $\mathbf{J}^{PO}$ is described as

$$\mathbf{J}^{PO} = \hat{\mathbf{n}} \times (\mathbf{H}_{i1} + \mathbf{H}_{r1}) \mid_S \simeq 2\hat{\mathbf{n}} \times \mathbf{H}_{i1} \mid_S . \quad (4.21)$$

Also, physical optics approximation supposes, when the geometry is in-

finite, PO current density is zero at all regions that are not directly illuminated by the source. This assumption will accelerate the computations of the surface current done by MoM. For our scenario, where a square plate is located above a rough surface, and both are illuminated by a plane wave, we would apply PO approximation to calculate the magnetic current on both two surfaces. From the results we have from the previous section, the zeroth order of the E-PILE method ($\mathbf{Y}^0$) can be written as

$$\begin{cases} \mathbf{Y}_1^0 = \bar{\mathbf{Z}}_1^{-1}(\mathbf{b}_1 - \bar{\mathbf{Z}}_{21}\bar{\mathbf{Z}}_2^{-1}\mathbf{b}_2), p = 0 \\ \mathbf{Y}_1^{(p)} = \bar{\mathbf{M}}_{c,1}\mathbf{Y}_1^{(p-1)}, p > 0 \end{cases} \tag{4.22}$$

where $\mathbf{b}_1 = \hat{\mathbf{n}}_1(\mathbf{R}_1) \times \mathbf{H}^i(\mathbf{R}_1)$ and $\mathbf{b}_2 = \hat{\mathbf{n}}_2(\mathbf{R}_2) \times \mathbf{H}^i(\mathbf{R}_2)$ are the tangential incident fields on scatterer 1 and scatterer 2 respectively. From the previous equation, the excitation can be divided into two sources, the first is from the direct illumination of the incident field $\mathbf{b}_1$, and the second source represented by $\bar{\mathbf{Z}}_{21}\bar{\mathbf{Z}}_2^{-1}\mathbf{b}_2$ is due to the coupling between the two scatterers, where $\bar{\mathbf{Z}}_2^{-1}\mathbf{b}_2$ represents the surface current density on the second scatterer alone without the effect of the other scatterer. Now, applying the PO principle and keeping in mind that $\mathbf{J}^{PO} = 2\hat{\mathbf{n}}(\mathbf{R}) \times \mathbf{H}^i(\mathbf{R})$,for $\mathbf{H}^i = 1$, the diagonal elements of the $\bar{\mathbf{Z}}^{-1}$ are equal to 2, where a direct illumination occurs and zero at the other regions (no point to point interaction at PO approximation), in other words, $\bar{\mathbf{Z}}_2^{-1}$ can be represented by $2\bar{\mathbf{I}}$, where $\bar{\mathbf{I}}$ is the identity matrix.

However, $\bar{\mathbf{Z}}_1^{-1}\mathbf{b}_1$ represents the surface current density at the first scatterer as if it is in the free space. When applying PO approximation, the diagonal of the $\bar{\mathbf{Z}}_1^{-1}$ is equal to 2 in the region of direct illumination, while the other elements of the matrix are zeros. That leads to accelerating the computations because there is no necessary to compute the inverse of $\bar{\mathbf{Z}}_1, \bar{\mathbf{Z}}_2$. For our scenario applying PO on the two scatterers is discussed in details as follows.

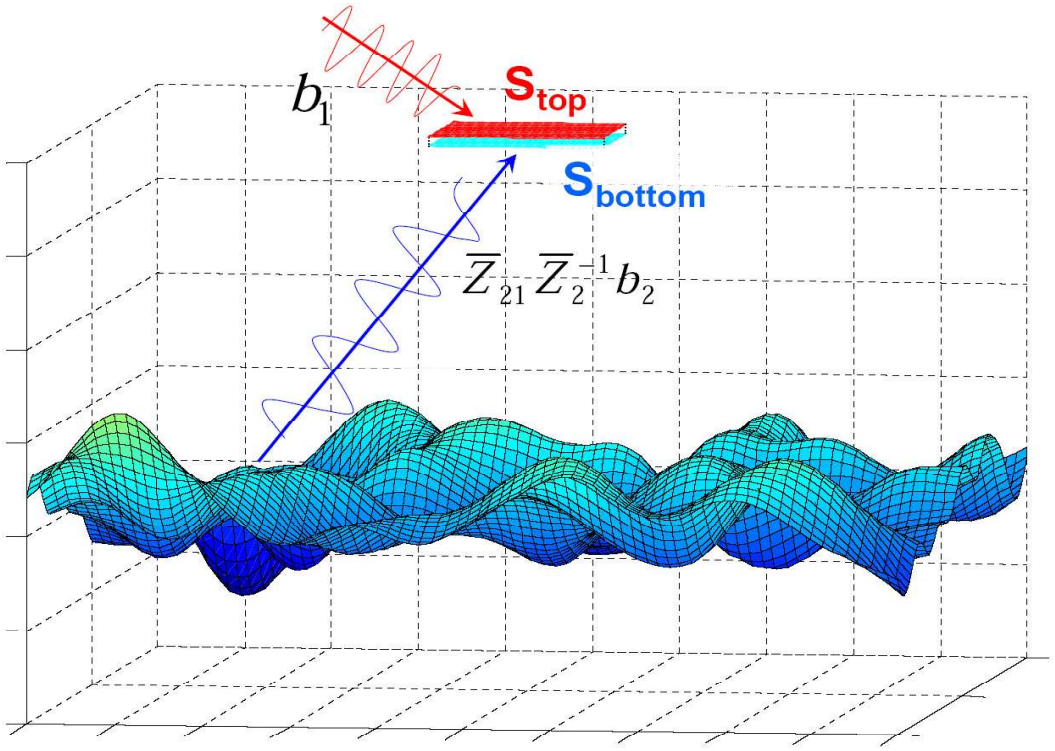

Figure 4.9: The excitation at the first scatterer by a plan wave.

To apply PO on the first scatterer, we should identify the regions of direct illumination and the shadowed regions. Figure 4.9 explain the illuminated and the shadowed regions.

As shown in Figure 4.9, we can consider the top side of the plat (S^{top}) as the region of the direct illumination from the plane wave $\mathbf{b}_1$, moreover,

the bottom side of the plate (S^{bottom}) is illuminated by the scattered field from the rough surface($\bar{\mathbf{Z}}_{21}\bar{\mathbf{Z}}_2^{-1}\mathbf{b}_2$), as a result, $\mathbf{b}_1$ becomes

$$\mathbf{b}_1' = \begin{bmatrix} \mathbf{b}_1^{top} \\ \mathbf{b}_1^{bottom} \end{bmatrix} \tag{4.23}$$

where $\mathbf{b}_1^{top}$ is the incident field at the first scatterer and equals to

$$\mathbf{b}_1^{top} = \begin{bmatrix} \hat{\mathbf{n}} \times \mathbf{H}^i(\mathbf{R}_1^1) \\ \hat{\mathbf{n}} \times \mathbf{H}^i(\mathbf{R}_1^2) \\ \vdots \\ \hat{\mathbf{n}} \times \mathbf{H}^i(\mathbf{R}_1^{N_{top}}) \end{bmatrix} \tag{4.24}$$

and $\mathbf{b}_1^{bottom}$ is the incident field at the bottom part of the plate, which is zero, $\mathbf{b}_1^{bottom}$ is describes as

$$\mathbf{b}_1^{bottom} = \begin{bmatrix} 0 \\ 0 \\ \vdots \\ 0 \end{bmatrix} \tag{4.25}$$

the dimension of $\mathbf{b}_1^{bottom}$ is $N^{bottom} \times 1$, where N^{top} and N^{bottom} are the number of the segments used in the top and bottom sides respectively. However, the coupling matrix $\bar{\mathbf{Z}}_{21}$ also modified as

$$\bar{\mathbf{Z}}_{21}' = \begin{bmatrix} \bar{\mathbf{Z}}_{21}^{top} \\ \bar{\mathbf{Z}}_{21}^{bottom} \end{bmatrix} \tag{4.26}$$

where $\bar{\mathbf{Z}}_{21}^{top}$ is the coupling matrix between the top side of the plate and the rough surface, and $\bar{\mathbf{Z}}_{21}^{bottom}$ is the coupling matrix between the bottom side of the plate and the rough surface. Since the scattered field from the rough surface illuminates the bottom side of the plate only, the elements of $\bar{\mathbf{Z}}_{21}^{top}$ are equals to zero, that because no reflected fields reach it. To summarize, equation 4.22 becomes

$$\begin{cases} \mathbf{Y}_1^0 = 2(\mathbf{b}_1' - \bar{\mathbf{Z}}_{21}' 2\mathbf{b}_2), for \quad p = 0 \\ \mathbf{Y}_1^{(p)} = \bar{\mathbf{M}}_{c,1}' \mathbf{Y}_1^{(p-1)}, for \quad p > 0 \end{cases} \tag{4.27}$$

where $\bar{\mathbf{M}}_{c,1}' = 2\bar{\mathbf{Z}}_{21}' 2\bar{\mathbf{Z}}_{12}$.

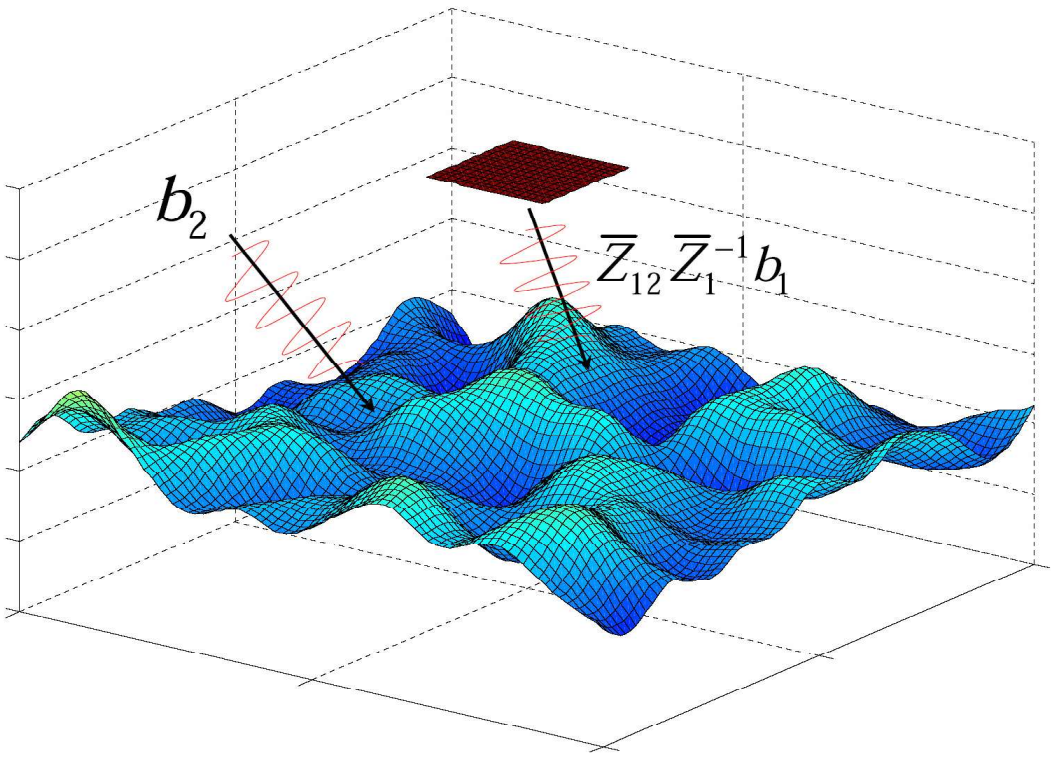

Figure 4.10: The excitation at the second scatterer by a plan wave.

Similarly, when we apply PO approximation on the second scatterer, the rough surface is illuminated by two fields, as shown in Figure 4.10, the di-

rect incident field ($\mathbf{b}_2$) and the scattered field from the first scatterer($\bar{\mathbf{Z}}_{12}\bar{\mathbf{Z}}_1^{-1}\mathbf{b}_1'$), these two fields hit the same side of the rough surface. The currents on the rough surface are calculated by

$$\begin{cases} \mathbf{Y}_2^0 = 2(\mathbf{b}_2' - \bar{\mathbf{Z}}_{12}'2\mathbf{b}_1), for \quad p = 0 \\ \mathbf{Y}_2^{(p)} = \bar{\mathbf{M}}_{c,2}'\mathbf{Y}_2^{(p-1)}, for \quad p > 0 \end{cases} \tag{4.28}$$

where $\bar{\mathbf{M}}_{c,2}' = 2\bar{\mathbf{Z}}_{12}2\bar{\mathbf{Z}}_{21}'$. To summarize, after applying PO approximation at the two scatterers, the equations of the currents and the characteristic matrix are reduced significantly, there is no necessary to calculate $\bar{\mathbf{Z}}_1^{-1}$ and $\bar{\mathbf{Z}}_2^{-1}$, this reduces the time and the memory used. The complexity of the inversion $\mathbf{O}(N_1^3)$ becomes 1 and $\mathbf{O}(N_2^3) \rightarrow 1$.

For our scenario of a square plate located above rough surface, consider the plate is of dimension of $1\lambda_0 \times 1\lambda_0$ and the rough surface of dimension $8\lambda_0 \times 8\lambda_0$, the two scatterers are separated by distance of $5\lambda_0$, and illuminated by plane wave at an incident angle of $\theta_i = 0^o$.

Figure 4.11 shows a comparison between the RCS of the MoM-LU and E-PILE of order 6 and the E-PILE of order 6 + PO at the two scatterers. The results in figure 4.11 shows that the RCS from E-PILE and E-PILE+PO1+PO2 are very similar for most scattering angles, the error between the two radar cross sections is very acceptable.

PO accelerated the computations and reduced the used memory. Recently, a very attractive method to accelerate the computations called

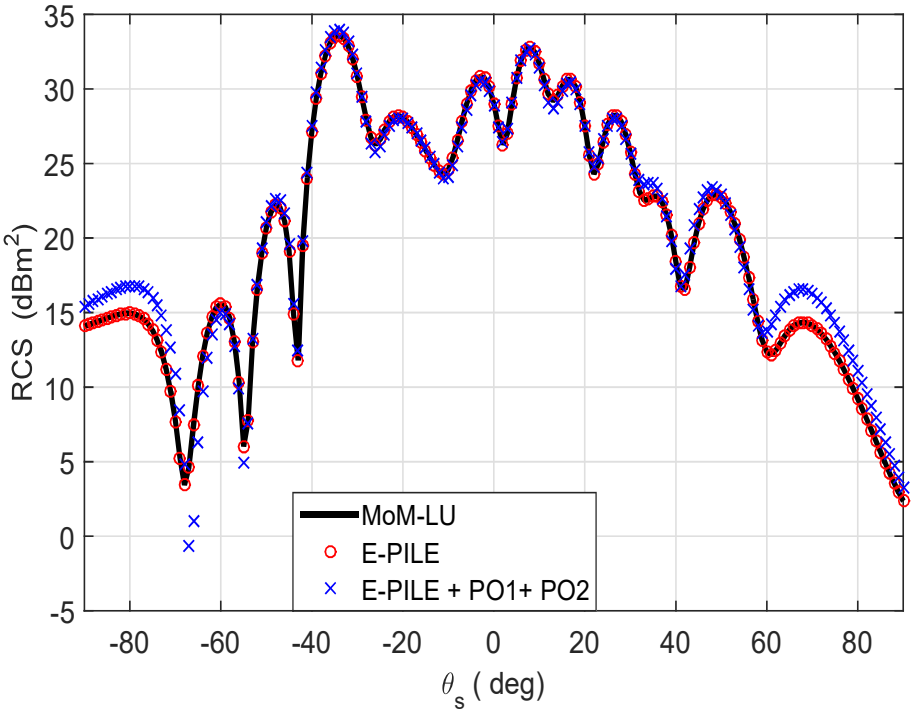

Figure 4.11: The RCS of plate above rough surface computed by MoM-LU, E-PILE, and E-PILE+PO1+PO2, the two scatterers are at dimensions of $1\lambda_0 \times 1\lambda_0$ and $8\lambda_0 \times 8\lambda_0$, separated by distance of $5\lambda_0$, and illuminated by plane wave at an incident angle of $\theta_i = 0^o$.

Adaptive Cross Approximation (ACA) is developed. ACA will be discussed in the following section.

4.5 Adaptive Cross Approximation

In the previous section, we used PO approximation to accelerate the computations on both surfaces. In this section, we will introduce the ACA and discuss how to use it to accelerate the computations of the coupling occurs between the two scatterers.

ACA is first introduced in [30], it proposed an adaptive method to approximate matrix by a multiplication of two approximated rectangular

matrices. From that time, ACA was widely used for several reasons, one of them is its pure algebraic structure, that makes ACA easily used with other exists methods without any changes in that methods structure. Moreover, using ACA, as we will discuss later, does not need full pre-knowledge of the matrix, in other words, there is no necessary to compute all elements of the matrix, ACA chooses some elements to approximate the whole matrix, these are the only elements to be calculated.

In summary, ACA gives the advantage of reducing the computations time and the used memory.

The impedance matrix occurs from applying E-PILE discretized by MoM consists of blocks of sub-matrices, $\bar{\mathbf{Z}}_1$ and $\bar{\mathbf{Z}}_2$ refer to the interaction occurs on the scatterer itself, while $\bar{\mathbf{Z}}_{12}$ and $\bar{\mathbf{Z}}_{21}$ are occurred because of the coupling between the two scatterers. This coupling sub-matrices will be reduced using ACA as will be shown later, due to the nature of the green functions used in MoM, and for two good separated scatterers, the coupling matrices can be represented by a much-reduced number of columns and rows.

To have a clear understanding about ACA, consider matrix $\bar{\mathbf{Z}}$ with dimensions $m \times n$, ACA approximates $\bar{\mathbf{Z}}^{m\times n}$ by a new matrix $\tilde{\bar{\mathbf{Z}}}^{m\times n}$, the approximated matrix is a multiplication of two rectangular matrices $\bar{\mathbf{V}}, \bar{\mathbf{U}}$, in the form of [30]

$$\tilde{\bar{\mathbf{Z}}}^{m\times n} = \bar{\mathbf{U}}^{m\times r}\bar{\mathbf{V}}^{r\times n} = \sum_{i=1}^{r} \mathbf{u}_i^{m\times 1}\mathbf{v}_i^{1\times n}, \tag{4.29}$$

where $\bar{\mathbf{U}}, \bar{\mathbf{V}}$ are rectangular matrices, r is the effective rank of the matrix $\bar{\mathbf{Z}}^{m\times n}$, $\mathbf{u}_i$ is the i^{th} row of the matrix $\bar{\mathbf{U}}$, and $\mathbf{v}_i$ is the i^{th} column of the matrix $\bar{\mathbf{V}}$. From that equation, since the rank of the matrix is less than or equals to the minimum dimension of the matrix ($r \leqslant min(m,n)$), the ACA takes its importance. Instead of save an impedance with $m \times n$ entities, ACA provides a $((m+n)\times r)$ elements to be saved, this is very efficient when we deal with matrices of large sizes.

If we suppose $\bar{\mathbf{R}}$ to be the error matrix between the impedance matrix ($\bar{\mathbf{Z}}$) and the approximated matrix ($\tilde{\mathbf{Z}}$), then the ACA aims to achieve

$$\left\|\bar{\mathbf{R}}^{m\times n}\right\| = \left\|\bar{\mathbf{Z}}^{m\times n}\right\| - \left\|\tilde{\mathbf{Z}}^{m\times n}\right\| \leqslant \varepsilon \left\|\bar{\mathbf{Z}}^{m\times n}\right\| \tag{4.30}$$

Where ε is a given tolerance, $\|\bullet\|$ denotes the matrix Frobenus norm, which is calculated by the square root of the sum of the absolute squares of the matrix elements. The choice of the ε depends on the application and the required accuracy of the results. After determining the value of ε, ACA starts to generate $\bar{\mathbf{U}}$ and $\bar{\mathbf{V}}$. The matrices $\bar{\mathbf{U}}$ and $\bar{\mathbf{V}}$ are constructed by selecting rows and columns from the $\bar{\mathbf{Z}}$ matrix, while $\bar{\mathbf{U}}$ and $\bar{\mathbf{V}}$ are generated, the algorithm generates an approximate error matrix $\tilde{\mathbf{R}}$, which is equal to $\left\|\bar{\mathbf{Z}} - \tilde{\mathbf{Z}}\right\|$, each time a new row or column of $\bar{\mathbf{Z}}$ is chosen, the corresponding error vector(row or column) is calculated by subtracting the actual column or row vector from the corresponding column or row vector of the approximate matrix that has been constructed in the previous iteration. The key point of choosing row or column re-

turns to the index where the largest enter of the last computed error column or vector is located. At the end of ACA algorithm, the two matrices U and V are filled, ACA is terminated when the following condition is satisfied

$$\left\|\bar{\mathbf{R}}\right\| \leqslant \varepsilon \left\|\bar{\mathbf{Z}}\right\|. \tag{4.31}$$

Since the full known of $\bar{\mathbf{Z}}$ is not necessary, ACA provides an estimation to the norm of $\bar{\mathbf{Z}}$ when computing the error matrix $\bar{\mathbf{R}}$, the norm of the error matrix is estimated after the k^{th} iteration as

$$\left\|\bar{\mathbf{R}^{(k)}}\right\| \simeq \left\|\bar{\mathbf{U}}_k\right\| \left\|\bar{\mathbf{V}}_k\right\|, \tag{4.32}$$

also [30]

$$\begin{aligned} \left\|\bar{\mathbf{Z}}\right\|^2 \simeq \left\|\tilde{\mathbf{Z}}\right\|^2 = \left\|\bar{\mathbf{U}}^{(k)}\right\|^2 \left\|\bar{\mathbf{V}^{(k)}}\right\|^2 = \left\|\tilde{\mathbf{Z}}^{(k-1)}\right\|^2 \\ +2\sum_{j=1}^{k-1} \left|\mathbf{u}_j^T \mathbf{u}_k\right| \cdot \left|\mathbf{v}_j \mathbf{v}_k^T\right| + \left\|\mathbf{u}_k\right\|^2 \left\|\mathbf{v}_k\right\|^2, \end{aligned} \tag{4.33}$$

Recall that the characteristic impedance we have after applying PO approximation is in the form

$$\begin{cases} \mathbf{Y}_1^0 = 2(\mathbf{b}_1' - \bar{\mathbf{Z}}_{21}' 2\ \mathbf{b}_2), for \quad p = 0 \\ \mathbf{Y}_1^{(p)} = \bar{\mathbf{M}}_{c,1}' \mathbf{Y}_1^{(p-1)}, for \quad p > 0 \end{cases} \tag{4.34}$$

and $\bar{\mathbf{M}}_{c,1}' = 2\bar{\mathbf{Z}}_{21}' 2\bar{\mathbf{Z}}_{12}$. We will apply ACA to approximate the coupling matrices $\bar{\mathbf{Z}}_{12}$ and $\bar{\mathbf{Z}}_{21}$, then the calculations of $\mathbf{X}_1^0, \mathbf{X}_2^0, \bar{\mathbf{M}}_{c,1}'$ and $\bar{\mathbf{M}}_{c,2}'$ using this approximation will significantly accelerate the time needed

and the memory used in our computations.

To implement the proposed method, consider the scenario of plate of dimension $1\lambda_0 \times 1\lambda_0$ is located above rough surface of dimension $8\lambda_0 \times 8\lambda_0$. The two scatterers are separated by distance of $5\lambda_0$. The RCS of the proposed method (E-PILE+PO1+PO2+ACA) is compared with the RCS for the previous methods (E-PILE and E-PILE +PO1+PO2) for three cases as follow:

case 1 : the plane wave is normal incidence (the incident angle is 0^o), the results is shown in Figure 4.12.

case 2 : the plane wave is horizontally polarized and the incident angle is 45^o, the results is shown in Figure4.13.

case 3 : the plane wave is vertically polarized and the incident angle is 45^o, the results is shown in Figure4.14.

As shown in the previous results, the proposed method shows almost the same RCS of the E-PILE method combined with PO applied on the both scatterers for most scattered angles.

As discussed in this section, ACA accelerates the computations and reduced the required time compared with the computation times needed from the methods we discussed in this thesis. We measured the time required for the MoM-LU, E-PILE+PO1+PO2 and E-PILE+PO1+PO2+ACA, we run the programs several times then take the average time needed. The computations were hold for a fixed size of rough surface of $5\lambda_0 \times 5\lambda_0$,

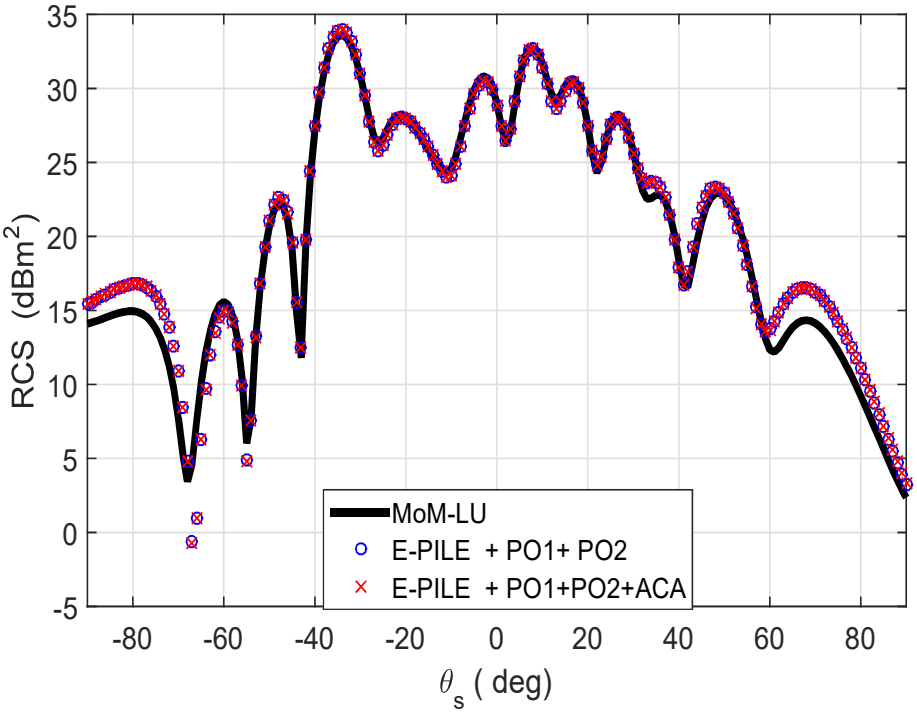

Figure 4.12: The RCS of plate above rough surface computed by MoM-LU, E-PILE+PO1+PO2 and and the proposed method E-PILE+PO1+PO2+ACA. The two scatterers are at dimensions of $1\lambda_0 \times 1\lambda_0$ and $8\lambda_0 \times 8\lambda_0$, separated by distance of $5\lambda_0$, and illuminated by a horizontally polarized plane wave at an incident angle of $\theta_i = 0^o$.

then we changed the size of the plate from $1\lambda_0 \times 1\lambda_0$ to $4\lambda_0 \times 4\lambda_0$. Figure 4.15 shows comparison between the time required for the MoM-LU, E-PILE+PO1+PO2 and E-PILE+PO1+PO2+ACA. From Figure 4.15, we can notice that using the ACA allows us to reduce the computing time significantly. In deeper look, at plate size of $5\lambda_0$ ACA approximately decreases the time 60 percent compared with the time MoM-LU takes. Also, the RCS from applying PO is almost the same as the RCS from PO combined with ACA, but the time used in PO combined with ACA is clearly less than time used in PO only. The effect of ACA appears clearly for more geometry sizes where the unknowns are huge.

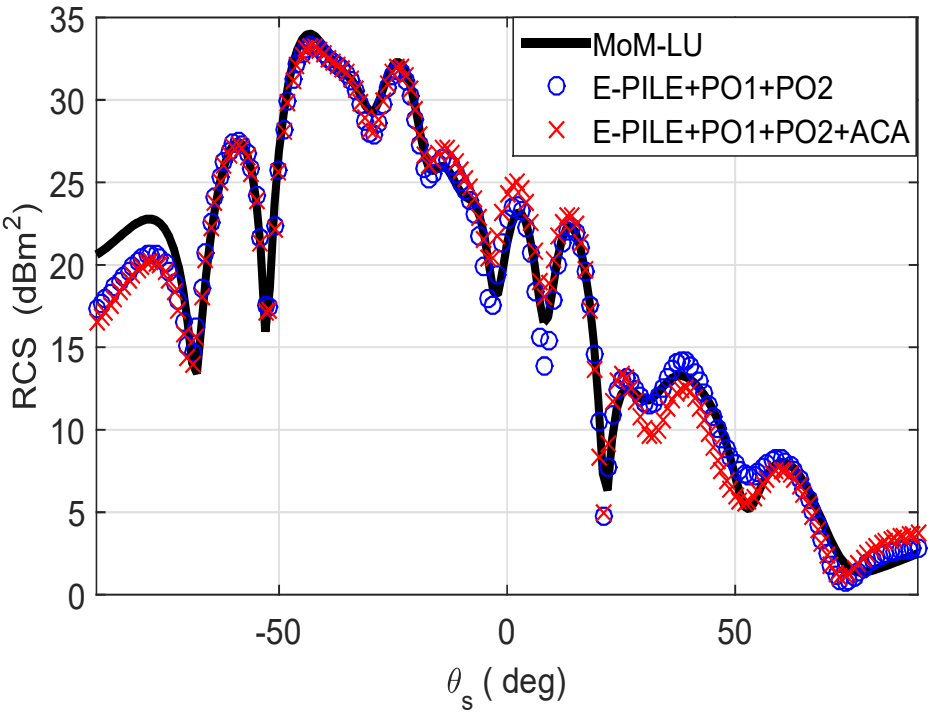

Figure 4.13: The RCS of plate above rough surface computed by MoM-LU, E-PILE+PO1+PO2 and the proposed method E-PILE+PO1+PO2+ACA. The two scatterers are at dimensions of $1\lambda_0 \times 1\lambda_0$ and $8\lambda_0 \times 8\lambda_0$, separated by distance of $5\lambda_0$, and illuminated by a horizontally polarized plane wave at an incident angle of $\theta_i = 45^o$.

4.6 Conclusion

In this chapter, the scattering between two scatterers is discussed. Then MoM as an exact method to calculate the RCS is applied. Then we applied PO approximation to accelerate the local interaction occurs at each scatterer, then we applied our proposed method (E-PILE+PO1+PO2+ACA) to accelerate the computations occurs on the coupling between the two scatterers. Finally, the required time needed from each method is measured and presented, the results shows reduction in time provided by the proposed method.

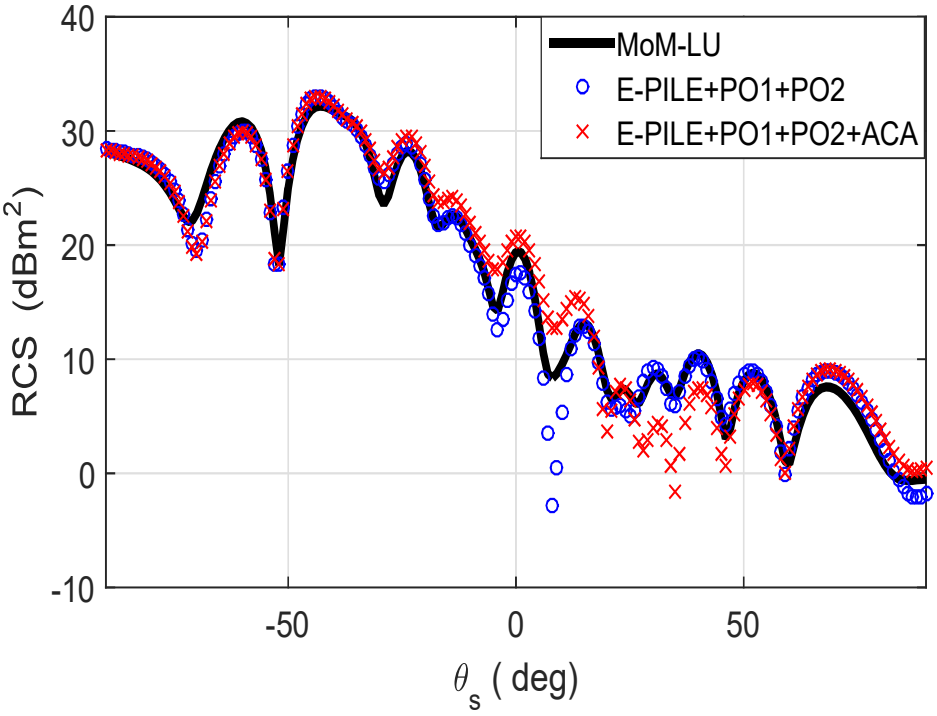

Figure 4.14: The RCS of plate above rough surface computed by MoM-LU, E-PILE +PO1 +PO2 and and the proposed method E-PILE +PO1 +PO2 +ACA. The two scatterers are at dimensions of $1\lambda_0 \times 1\lambda_0$ and $8\lambda_0 \times 8\lambda_0$, separated by distance of $5\lambda_0$, and illuminated by a vertically polarized plane wave at an incident angle of $\theta_i = 45^o$.

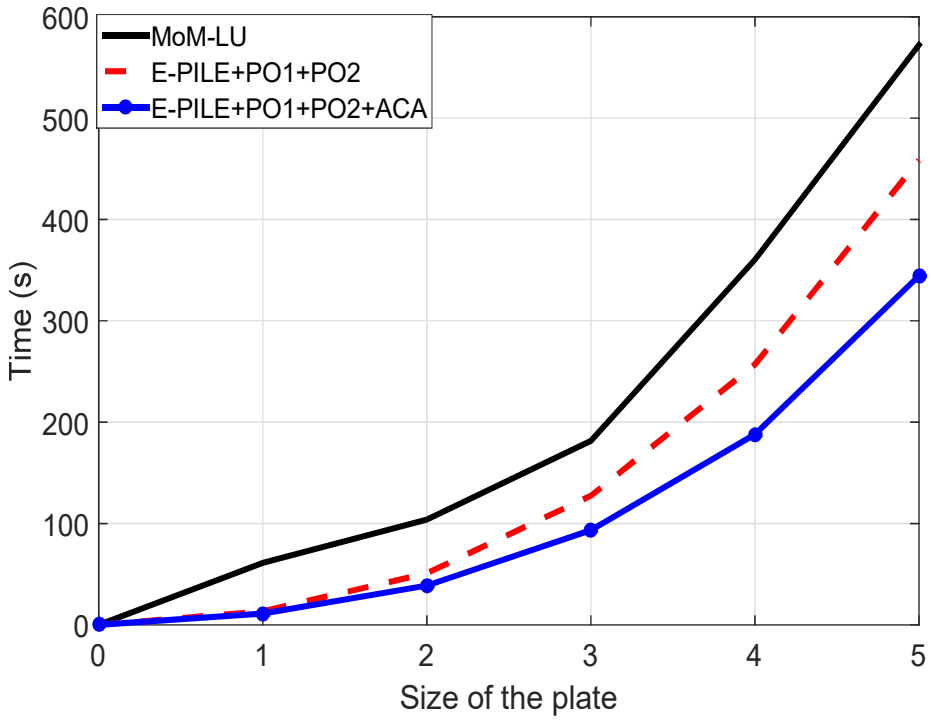

Figure 4.15: Comparison of time requires for the three methods, MoM-LU, E-PILE combined with PO and E-PILE combined with PO accelerated by ACA. The time is for scenario of square plate of dimensions from $1\lambda_0 \times 1\lambda_0$ to $4\lambda_0 \times 4\lambda_0$ and the rough surface is in the dimension of $5\lambda_0 \times 5\lambda_0$.

Chapter 5

Conclusion and Future Work

5.1 Conclusion

In this thesis, we discussed the scattering phenomenon for one scatterer in two cases, electrostatic and scattering cases. MoM was applied to solve the integral equations on two examples (thin wire and square plate). Then the concept of MoM was applied on electrodynamic cases such as an isolated square plate and rough surface illuminated by a plane wave, in each case the RCS is computed and discussed.

Later, we discussed the scattering occurred between two scatterers, we discretized the two scatterers using MoM, then PO approximation was applied to approximate the surface current on both two scatterers, then the ACA was combined to accelerate the computations of the coupling occurs between the two scatterers.

The proposed method (E-PILE+PO1+PO2+ACA) was applied and tested on a scenario of a square plate located above a rough surface. The results were attractive, the computed RCS from the proposed method was very similar to RCS from the E-PILE+PO for most scattering angles. Also, the proposed method (E-PILE+PO1+PO2+ACA) reduced

the complexity of the system, this was clearly appeared by the reduction in time that the proposed methods provided. This makes the proposed method suitable for applications deals with large objects.

5.2 Future Work

In a future development of the proposed method, we suggest using computers with better specifications to take results for larger scenarios. The proposed method could be applied to study scattering occurs in a scenario of more than two scatterers. Moreover, it is possible to use other integral equations and apply our method in a case of two dielectric media instead of PEC discussed in this thesis.

Bibliography

[1] Kong JA. Electromagnetic wave theory. EMW Publishing, Massachusetts, USA, 18-23, 2005.

[2] Taflove A, Hagness SC. Computational electrodynamics: the finite-difference time-domain method. Artech house, 2005.

[3] Kunz KS, Luebbers RJ. The finite difference time domain method for electromagnetics. CRC press; 1993 May 3.

[4] J. Jin, "The Finite Element Method in Electromagnetics", Wiley and Sons, 1993.

[5] Volakis JL, Chatterjee A, Kempel LC. Finite element method electromagnetics: antennas, microwave circuits, and scattering applications. John Wiley and Sons; 1998 Jun 15.

[6] Gibson WC. The method of moments in electromagnetics. Chapman and Hall/CRC; 2007 Nov 28.

[7] Keller JB. Geometrical theory of diffraction. JOSA. 1962 Feb 1;52(2):116-30.

[8] Kouyoumjian RG, Pathak PH. A uniform geometrical theory of diffraction for an edge in a perfectly conducting surface. November. 1974 Nov 1;88:1448-61.

[9] Balanis CA. Advanced engineering electromagnetics. John Wiley and Sons; 1999.

[10] Guo LX, Wang AQ, Ma J. Study on EM scattering from 2-D target above 1-D large scale rough surface with low grazing incidence by parallel MoM based on PC clusters. Progress In Electromagnetics Research. 2009;89:149-66.

[11] Liu P, Jin YQ. The finite-element method with domain decomposition for electromagnetic bistatic scattering from the comprehensive model of a ship on and a target above a large-scale rough sea surface. IEEE Transactions on Geoscience and Remote Sensing. 2004 May;42(5):950-6.

[12] Ye H, Jin YQ. A hybrid analytic-numerical algorithm of scattering from an object above a rough surface. IEEE Transactions on Geoscience and Remote Sensing. 2007 May;45(5):1174-80.

[13] Dechamps, N., N. De Beaucoudrey, C. Bourlier, and S. Toutain, "Fast numerical method for electromagnetic scattering by rough layered interfaces: Propagation-inside-layer expansion method", Journal of the Optical Society of America A, Vol. 23, 359-369, 2006.

[14] Déchamps N, de Beaucoudrey N, Bourlier C, Toutain S. Fast numerical method for electromagnetic scattering by rough layered interfaces: Propagation-inside-layer expansion method. JOSA A. 2006 Feb 1;23(2):359-69.

[15] Pino MR, Obelleiro F, Landesa L, Burkholder RJ. Application of the fast multipole method to the generalized forward–backward iterative algorithm. Microwave and Optical Technology Letters. 2000 Jul 20;26(2):78-83.

[16] Kubicke G, Bourlier C. A fast hybrid method for scattering from a large object with dihedral effects above a large rough surface. IEEE Transactions on Antennas and Propagation. 2011 Jan;59(1):189-98.

[17] Pino MR, Landesa L, Rodriguez JL, Obelleiro F, Burkholder RJ. The generalized forward-backward method for analyzing the scattering from targets on ocean-like rough surfaces. IEEE Transactions on Antennas and Propagation. 1999 Jun;47(6):961-9.

[18] Ye H, Jin YQ. Fast iterative approach to difference scattering from the target above a rough surface. IEEE Transactions on Geoscience and Remote Sensing. 2006 Jan;44(1):108-15.

[19] Ye H, Jin YQ. A hybrid KA-MoM algorithm for computation of scattering from a 3-D PEC target above a dielectric rough surface. Radio Science. 2008 Jun 1;43(3).

[20] Guan B, Zhang JF, Zhou XY, Cui TJ. Electromagnetic scattering from objects above a rough surface using the method of moments with half-space Green's function. IEEE Transactions on Geoscience and Remote Sensing. 2009 Oct;47(10):3399-405.

[21] Johnson JT. A numerical study of scattering from an object above a rough surface. IEEE Transactions on Antennas and Propagation. 2002 Oct;50(10):1361-7.

[22] Johnson JT, Burkholder RJ. Coupled canonical grid/discrete dipole approach for computing scattering from objects above or below a rough interface. IEEE Transactions on Geoscience and Remote Sensing. 2001 Jun;39(6):1214-20.

[23] Johnson JT. A study of the four-path model for scattering from an object above a half space. Microwave and optical technology letters. 2001 Jul 20;30(2):130-4.

[24] Guo LX, Li J, Zeng H. Bistatic scattering from a three-dimensional object above a two-dimensional randomly rough surface modeled with the parallel FDTD approach. JOSA A. 2009 Nov 1;26(11):2383-92.

[25] Kuang L, Jin YQ. Bistatic scattering from a three-dimensional object over a randomly rough surface using the FDTD algorithm. IEEE Transactions on Antennas and Propagation. 2007 Aug;55(8):2302-12.

[26] Kouali M, Kubické G, Bourlier C. Extended propagation-inside-layer expansion method combined with the forward-backward method to study the scattering from an object above a rough surface. Optics letters. 2012 Jul 15;37(14):2985-7.

[27] Boag A, Mittra R. Complex multipole beam approach to electromagnetic scattering problems. IEEE transactions on antennas and propagation. 1994 Mar;42(3):366-72.

[28] Tap K, Pathak PH, Burkholder RJ. Complex source beam-moment method procedure for accelerating numerical integral equation solutions of radiation and scattering problems. IEEE Transactions on Antennas and Propagation. 2014 Apr;62(4):2052-62.

[29] Canning FX. The impedance matrix localization (IML) method for moment-method calculations. IEEE Antennas and Propagation Magazine. 1990 Oct;32(5):18-30.

[30] Zhao K, Vouvakis MN, Lee JF. The adaptive cross approximation algorithm for accelerated method of moments computations of EMC problems. IEEE transactions on electromagnetic compatibility. 2005 Nov;47(4):763-73.

[31] Kubicke G, Bourlier C, Bellez S, Li H. A fast EPILE+ FBSA method combined with adaptive cross approximation for the scattering from a target above a large ocean-like surface. Progress In Electromagnetics Research. 2014;37:175-82.

[32] Yang W, Qi C. A Bi-Iteration Model for Electromagnetic Scattering from a 3D Object above a 2D Rough Surface. Electromagnetics. 2015 Apr 3;35(3):190-204.

[33] Sadiku MN. Elements of electromagnetics. Oxford university press; 2014 Jan 29.

[34] Stratton JA. Electromagnetic theory. John Wiley and Sons; 2007 Jan 22.

[35] Kouali M, Kubicke G, Bourlier C. Diffusion d'une onde électromagnétique par un objet au-dessus d'une surface rugueuse. InGDR Ondes" Interaction des ondes éléctromagnétiques avec des cibles ou/et le milieu naturel" 2011 Jun 20.

[36] Bourlier C, Pinel N, Kubické G. Method of moments for 2D scattering problems: basic concepts and applications. John Wiley and Sons; 2013 Aug 5.

[37] Gibson WC. The method of moments in electromagnetics. Chapman and Hall/CRC; 2007 Nov 28.

[38] Altair SA Development S.A. (Pty) Ltd Stellenbosch. FEKO, Field Computations Involving Bodies of Arbitrary Shape, Suite 7.0, 2014.

[39] Kouali M, Kubické G, Bourlier C. Electromagnetic interactions analysis between two 3-D scatterers using the E-PILE method combined with the PO approximation. Progress In Electromagnetics Research. 2014;58:123-38.

تقنية لتسريع حساب تشتت الأمواج الكهرومغناطيسية بين أجسام ثلاثية الأبعاد

إعداد: نور ماجد محمد عبيد

إشراف :د.محمد كوعلي

ملخص:

في الآونة الأخيرة، ازدادت الأبحاث المتعلقة في تشتت الأمواج الكهرومغناطيسية عن الأجسام ثلاثية الأبعاد، ذلك لدخول تشتت الأمواج في الكثير من التطبيقات مثل الرادار و أنظمة الاستشعار عن بعد و في أنظمة الألياف الضوئية و غيرها، و لذلك وجدت العديد من الطرق التي اهتمت بدراسة هذه الظاهرة.

تقسم الطرق لدراسة ظاهرة تشتت الأمواج الكهرومغناطيسية إلى نوعين، يهتم النوع الأول في إيجاد حل دقيق لنظام المعادلات التكاملية المعقد، و من الأمثلة عليها (MoM)، بالرغم من حاجة بعض التطبيقات إلى النتيجة الدقيقة، إلا إن استخدامها مكلف جدا من ناحية متطلبات الذاكرة المستخدمة و الوقت اللازم لإظهار النتائج، مما يجعل هذه الطرق محدودة بحجم أجسام صغير. حديثا، ظهرت طريقة (E-PILE) التي قامت باقتراح لتسريع حسابات نظام (MoM) دون التأثير على دقة النتائج مما زاد في إمكانيات (MoM) في حل المعادلات لأجسام اكبر نسبيا.

يهتم النوع الثاني من الطرق بعمل تقريب للمعادلات التكاملية، مما يقلل من تعقيد الحسابات و يوفر الذاكرة و الوقت، بالمقابل تقل دقة النتائج المقدمة، و من هذه الطرق : طريقة الفيزياء البصرية (PO) التي تقوم على عدة افتراضات تؤدي بالنتيجة إلى تقليل تعقيد النظام و إعطاء نتائج بوقت اقل، و أيضا ظهرت مؤخرا طريقة جبرية تقوم على تسريع الحسابات الجبرية

للمصفوفات كبيرة الحجم تسمى (ACA).

في هذه الرسالة، تم استخدام (MoM) مدموجة بطريقة (E-PILE) لحساب الأمواج المشتتة بين جسمين (صفيحة مربعة فوق جسم غير منتظم (Rough Surface))، و تم استخدام تقريب (PO) لحساب التيار التقريبي على سطح الجسمين، و من ثم تسريع حسابات تأثير قرب الجسمين من بعضهما (Coupling) باستخدام (ACA).

تم حساب المقاطع الراداريوية (RCS) للطريقة المقترحة (E-PILE+PO+ACA) و الطريقة الدقيقة (MoM) و الناتجة عن دمج (E-PILE+PO) و مقارنتهم معا. و تم قياس الوقت اللازم لإجراء الحسابات و إظهار النتائج للطرق الثلاثة السابقة و مقارنتها معا.

أظهرت النتائج المعروضة وجود نسبة خطا مقبولة في المقطع الراداري الخاص بالطريقة المقترحة مقارنة مع باقي الطرق. كما أدى استخدام (ACA) إلى تقليل ملحوظ في التعقيد (Complexity)، ظهر تأثيره واضحا في تسريع الوقت اللازم لإجراء الحسابات.